AFOSR TN

THE UNIVERSITY OF MICHIGAN

DEPARTMENT OF AERONAUTICAL AND ASTRONAUTICAL ENGINEERING
Aircraft Propulsion Laboratory

AN EXPERIMENTAL AND THEORETICAL STUDY OF STATIONARY GASEOUS DETONATION WAVES

J.A. Nicholls
E.K. Dabora
R.B. Morrison
T.C. Adamson, Jr.
R.L. Phillips
A.A. Ranger
G.J. Lelli
G.L. Cosens

ORA Project 02874

under contract with:

PROPULSION RESEARCH DIVISION
AIR FORCE OFFICE OF SCIENTIFIC RESEARCH
OFFICE OF AEROSPACE RESEARCH
CONTRACT NO. AF 49(638)-562
WASHINGTON, D.C.

administered through:

OFFICE OF RESEARCH ADMINISTRATION ANN ARBOR

October 1961

ACKNOWLEDGMENT

This research was supported by the United States Air Force under Contract No. AF 49(638)-562, monitored by the Air Force Office of Scientific Research, Propulsion Research Division, Office of Aerospace Research. The support of this agency is gratefully acknowledged.

TABLE OF CONTENTS

LIST OF FIGURES

TABLE OF CONTENTS (Concluded)

I. INTRODUCTION

The work reported herein was effected under Air Force Office of Scientific Research Contract No. AF 49(638)-562 which covered the period 1 February 1959 through 31 October 1961. This contract represented a continuation of earlier work conducted under contract No. AF 18(600)-1109 which was summarized in a final report.[1]

Some of the theoretical and experimental findings have been previously reported in the literature and thus will not be discussed in detail herein. Any new work will, of course, be described in detail.

The major portion of this report (through Section VI entitled "Two Dimensional Effects") is devoted explicitly to the study of the standing detonation wave in a hydrogen-air mixture. The experimental arrangement and procedures employed are briefly described and the experimental results presented. A revised analysis of the ignition delay zone behind the shock is presented which handles the equations more rigorously than an earlier treatment. The prediction of the time rate of growth of concentrations of the radicals behind the shock is found to be slightly different than the earlier analysis[2] but the prediction of ignition time delay is unchanged. Vibrational relaxation is considered insofar as it affects the ignition time delay. Preliminary measurements aimed at probing the combustion region of the detonation wave by means of the sodium D-line reversal technique are described. A consideration of some probable two dimensional effects behind the shock reveal a likely explanation of some hitherto uncertain anomalous ignition delay measurements.

Two additional sections are also included. One is devoted to the theoretical prediction of magneto-gasdynamic effects on plane gaseous detonation waves and the other to an attempted experimental check on the linearized theory of heat addition in a supersonic stream.

II. EXPERIMENTAL ARRANGEMENT

The experimental setup has been described in detail in Ref. 2 and 3 and therefore only a brief description will be given here. High pressure air after having been heated by a regenerative type heat exchanger flows through an axisymmetric convergent divergent nozzle. The exit pressure is much higher than the receiver pressure (atmosphere), so that the open jet has the familiar jet structure shown schematically in Fig. 1. Hydrogen at room temperature but at a pressure corresponding to the throat pressure of the nozzle is introduced by a needle at the throat. Since the flow field downstream of the throat up to the Mach disc of the jet is expanding with the attendant drop in static temperature, no combustion occurs in this region. After the gaseous mixture passes through the Mach disc (i.e., through a normal shock), combustion becomes possible provided certain conditions of pressure and temperature are met, as will be explained later.

The experimental arrangement includes a continuous light source schlieren system and a 35 mm movie camera for the continuous photography of the jet structure as well as the combustion zone which is rendered visible by the introduction of a sodium compound with the hydrogen. The sodium compound is also used for the measurement of temperature by the D-line reversal method when possible. A schematic diagram of the schlieren and temperature measurement systems is shown in Fig. 2. Pressures and temperatures necessary for the determination of the flow rates of both the air and the hydrogen are measured at all times.

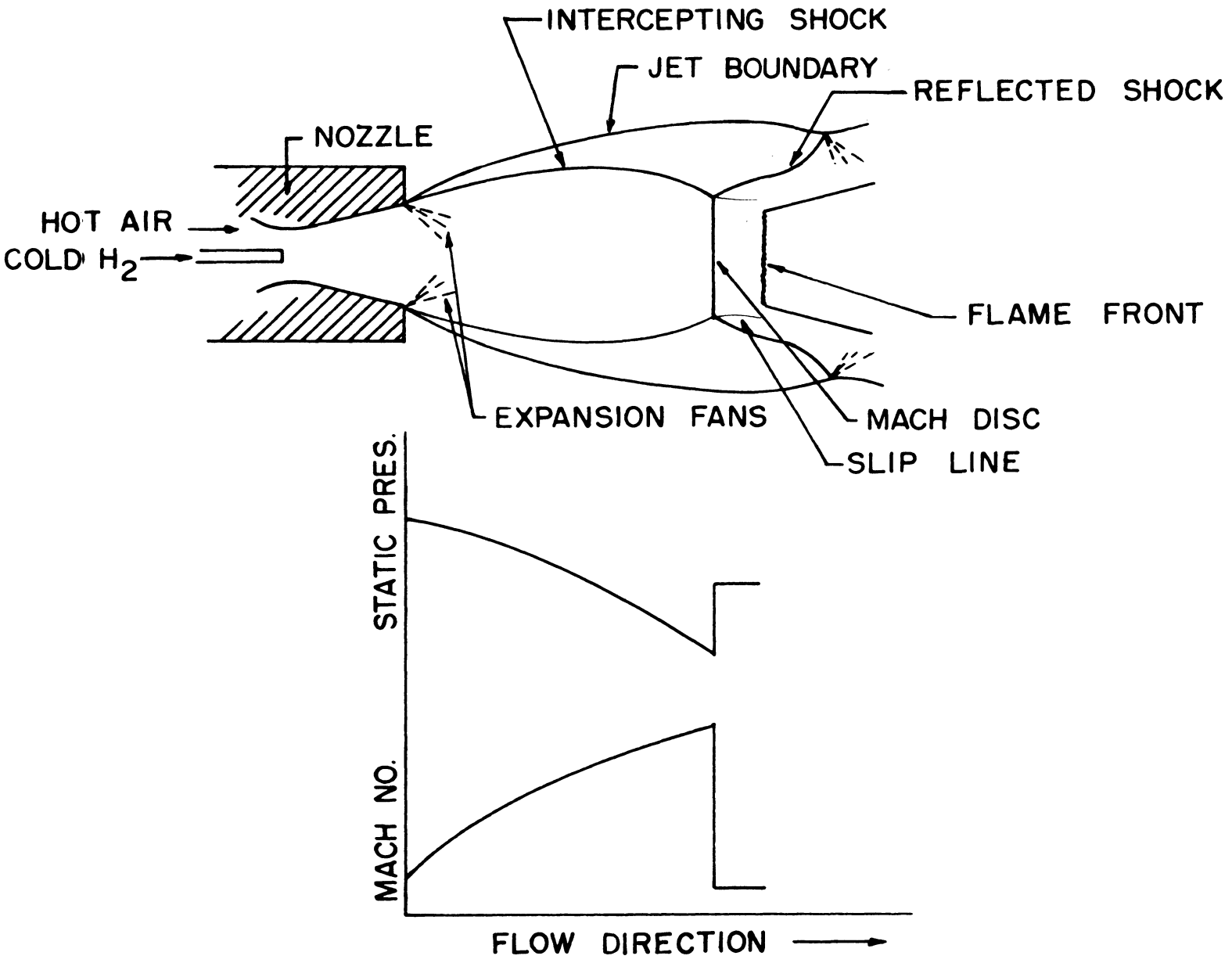

Fig. 1. Schematic of nozzle and jet structure.

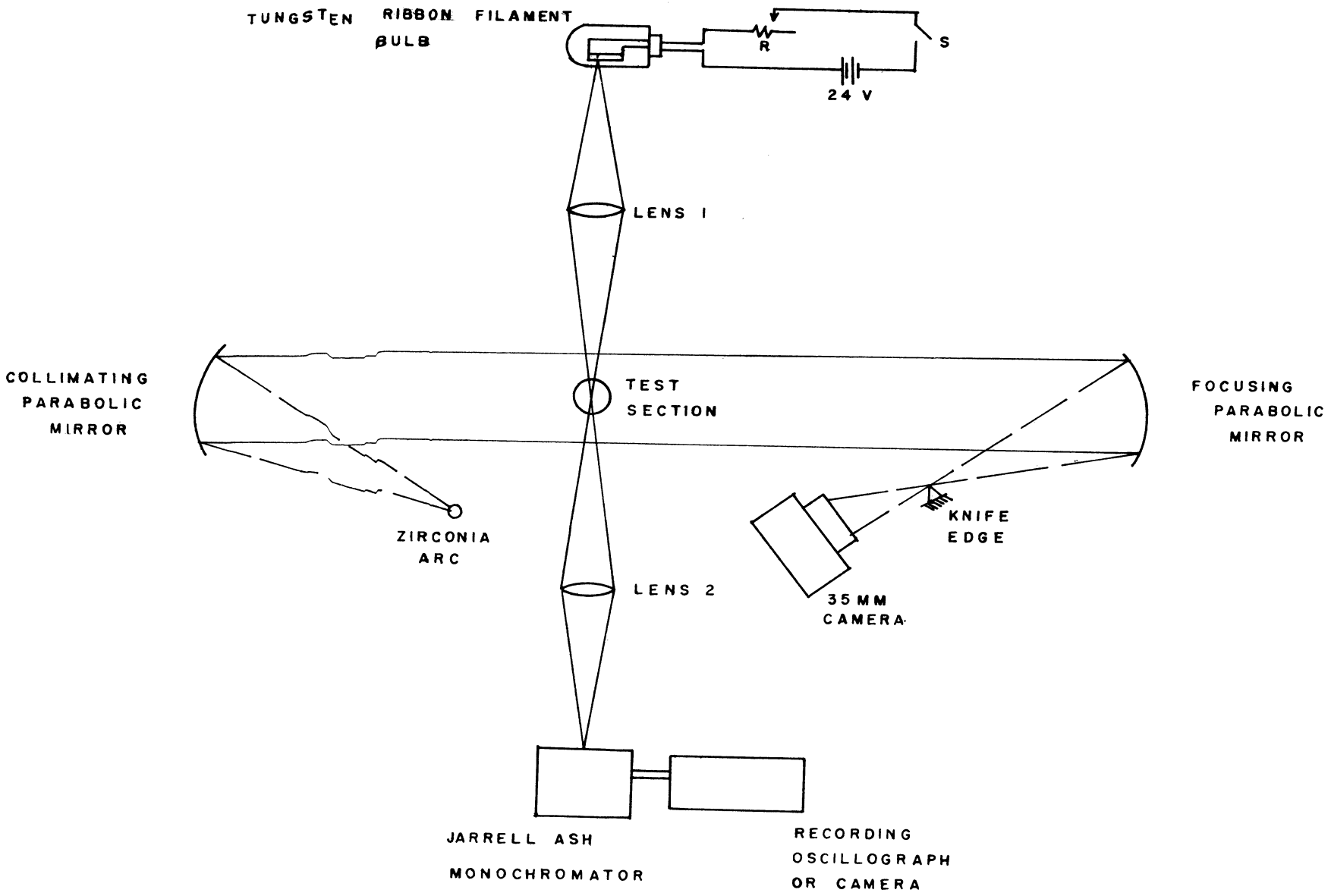

Fig. 2. Schematic diagram of schlieren system and the D-line reversal technique of temperature measurement.

A few experiments were also made in which the stagnation temperature of the air was increased by the addition of a small amount of hydrogen (preheat hydrogen). This was done for two reasons: one, to obtain stagnation temperature higher than that obtainable by the heat exchanger and two, to be able to vary the stagnation temperature by varying the preheat hydrogen during a particular experiment. The increase in temperature realized by this technique was limited to about 300°F as greater hydrogen additions led to premature burning within the nozzle. Experimental results obtained with hydrogen preheat were consistent with other results obtained.

The actual experimental data taken will be presented in the later sections when pertinent to the discussion.

III. TEMPERATURE MEASUREMENT BY THE SODIUM D-LINE REVERSAL METHOD

Flame temperatures have been successfully measured in the past by the sodium D-line technique.[4] It was therefore decided to adapt this technique to the measurement of the temperature of the flame region of the standing detonation wave. Before describing the actual experimental apparatus used, it is well to mention the underlying principle of the technique. Light from a tungsten filament bulb is focused on the flame. The flame which is contaminated by sodium or sodium compound as well as the image of the light source at the flame are focused at the entrance slit of the spectroscope. If the light source is turned off, the spectroscope would show the characteristic resonance lines of Na at 5890 and 5896Å. If only radiation from the light source is incident on the entrance slit, the spectroscope would show a continuous spectrum whose brightness depends on the temperature of the filament. Thus when both flame and light source are focused on the entrance slit, the D-lines would appear bright in a dark background or dark on bright background depending on whether the flame temperature is higher or lower than the brightness temperature of the image of the light source. If the light source temperature is varied, it is possible to find a case wherein the D-lines are indistinguishable from the continuous background. *Application of Kirchhoff's radiation law and Planck's or Wien's radiation* formula under this condition shows that the brightness temperature of the image of the light source at the flame location is equal to the flame temperature provided that the sodium particles are in thermal equilibrium

with the flame. More details on the technique are given in Refs. 5 and 6. The latter describes a self-balancing instrument which was used at NACA.

The components used in this study are as follows. The light source used was a ribbon filament type tungsten lamp model 18 AT 10 made by General Electric. Its intensity was varied by using a variable resistor in series with it. The power supply, which consisted of two heavy duty 12V truck batteries connected in series, provided a steady voltage. The focal length of the first lens which focuses the light source on the flame was 8.5 in. and that of the second one was 16 in. Insurance that all light rays from the flame falling on the spectroscope slit are superimposed by light rays originating from the light source is made by limiting the second lens so that its aperture ratio is somewhat smaller than that of the first. The spectroscope used was of the scanning type made by Jarrell Ash, Model 8200, which has a dispersion of 16Å/mm.

Two ways of recording the intensity of a narrow part of the spectrum (about 30Å span which included the D-lines) were employed. In the first one, light from the exit slit of the spectroscope falls on a photomultiplier whose output is recorded by a Consolidated 14 channel oscillograph. The scanning mechanism of the spectroscope was modified so that only the spectrum between 5882 and 5904Å is scanned in one cycle. At each cycle the intensity of the light source is kept constant. The current to the bulb is recorded on the oscillograph simultaneously with spectrum intensity. Thus the current to the bulb at which reversal occurs can be detected and from previous calibration the brightness temperature which corresponds to the flame temperature can be

obtained. Although this method was checked out with a Bunsen flame it met with difficulty when it was applied to the standing wave. Excessive "noise" was encountered in the intensity of the spectrum close to the D-lines and therefore the reversal point was hard to detect. The reasons for the noise could be temperature fluctuation of the flame and the relatively low temperature operation. Vibration of some components of the optical system due to the jet noise cannot be altogether discounted.

The second method adopted was to orient both the image of the ribbon filament and the spectroscope entrance slit parallel to the flow direction. A spectrum between 5880 and 5910Å is photographed by a 35 mm camera as it emerges from the exit slit which was left wide open. The light source is varied by varying the current to it which again was recorded on the oscillograph. Suitable timing marks on the photographic film and the oscillograph paper were employed to establish correspondence between the two. Now if the flame temperature varies along the axis within a distance equivalent to the slit length, then reversal would occur at different parts of the D-lines as the light intensity is varied. Thus it would be possible to measure in a single run the axial variation of the temperature. This method was tried and resulted in a detection of temperature close to the adiabatic flame temperature, without much variation within 1/4-in. axial distance. Further work utilizing this method was precluded when the lining of the heat exchanger burned out.

It should be pointed out that the reversal temperature obtained by the D-line technique is the correct temperature of the flame as long as the region contaminated by Na is uniform in temperature along the optical path. If this

is not the case, the reversal temperature indicates some average temperature. To measure temperature variation along the optical path a more exacting technique would have to be employed. Because such a technique was contemplated an outline of it is presented here as a guide for future work.

The method is based on Pearce's work,[7] and requires first a determination of the emissivity profile of the flame.

In order to obtain the emissivity profile two assumptions are made: (1) the temperature and emissivity in any axial plane is axisymmetric and (2) the emitter density i.e., the Na particle density is also axisymmetric.

Now, the radiation intensity at the D-line region of the spectrum is measured as a function of distance x from the axis of the flame once directly and another time after it has been reflected by a plane mirror of reflectivity r. Thus two curves would be obtained typified by those shown in Fig. 3. From these curves the emissivity profile is obtained. To do this, the flame area is divided into elements as shown in Fig. 3 with each element denoted by ΔA_{jk} where the index j denotes the x location of the elements and the index k denotes the radial location. Numerical values for ΔA_{jk}'s for j and k up to 25 are tabulated in Ref. 7. It is then assumed that the emissivity of each element is proportional to the number of emitters in each element, and thus for elements in the same radial location the emissivity is proportional to the area of the element [this is so because of assumption (2) above]. This implies that the element is thin enough so that no self-absorption is present within it. Now the direct intensity of the flame I_1 and the reflected intensity I_1' at x = 1 are related to each other as follows:

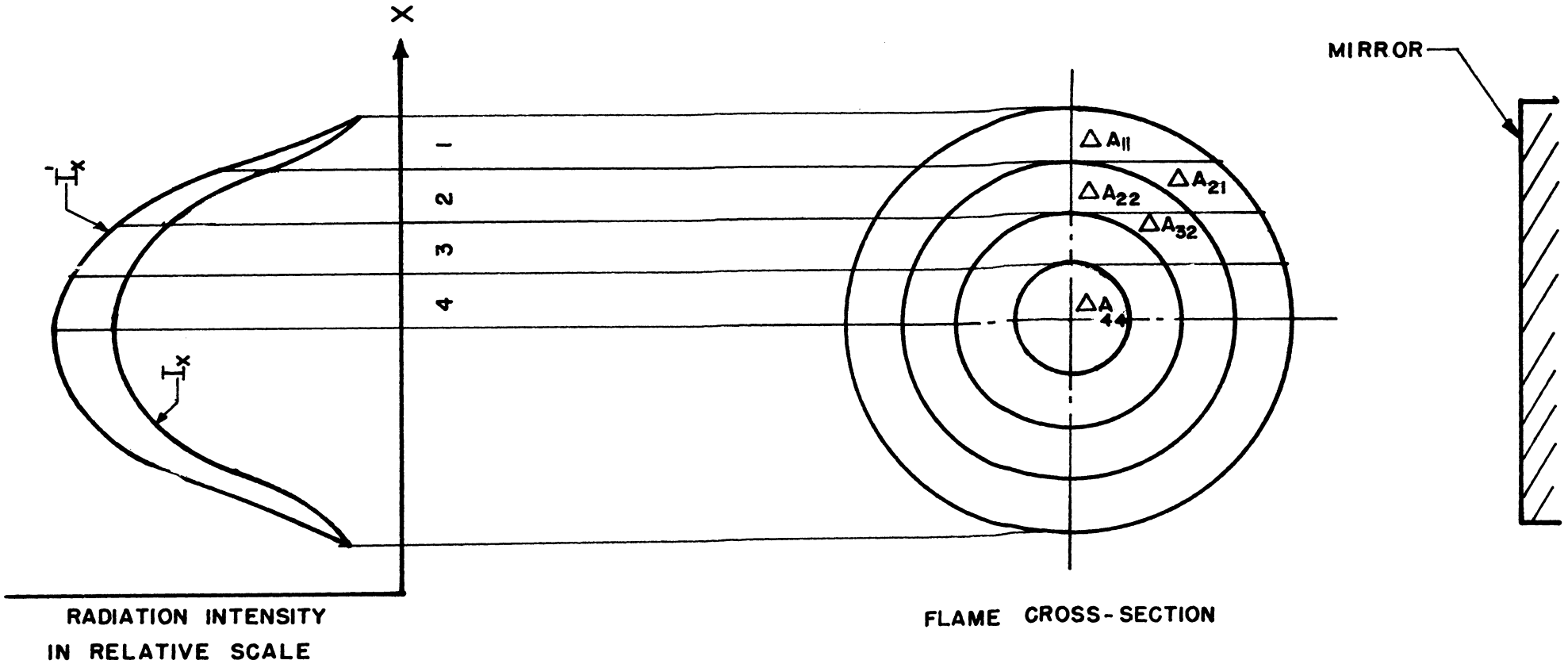

Fig. 3. Typical radiation intensity distribution for flame emissivity calculation (I_x without mirror, I_x' with mirror).

$$I_1' = I_1 + r\, I_1(1 - \epsilon_{11})(1 - \epsilon_{11}) \tag{3.1}$$

where ϵ_{11} is the emissivity of element ΔA_{11} and is of course equal to the absorptivity. With r and I_1'/I_1 known, ϵ_{11} can be calculated as

$$\epsilon_{11} = 1 - \left[\left(\frac{I_1'}{I_1} - 1\right)\frac{1}{r}\right]^{1/2} \tag{3.2}$$

Thus, the calculation of the emissivity does not depend on the absolute values of the intensities but only on their ratio.

Similarly one can write, for location x = 2:

$$I_2' = I_2 + r\, I_2(1 - \epsilon_{21})^2(1 - \epsilon_{22})^2 \tag{3.3}$$

but

$$\epsilon_{21} = \frac{\Delta A_{21}}{\Delta A_{11}}\,\epsilon_{11} \tag{3.4}$$

therefore

$$\epsilon_{22} = 1 - \left[\left(\frac{I_2'}{I_2} - 1\right)\frac{1}{r}\right]^{1/2}\left(\frac{1}{1 - \frac{\Delta A_{21}}{\Delta A_{11}}\,\epsilon_{11}}\right) \tag{3.5}$$

with ϵ_{11} known, ϵ_{22} can thus be obtained. In general one can write:

$$\epsilon_{jj} = 1 - \left[\left(\frac{I_j}{I_j} - 1\right)\frac{1}{r}\right]^{1/2} \frac{1}{\prod_{k=1}^{j-1}\left(1 - \frac{\Delta A_{jk}\,\epsilon_{kk}}{\Delta A_{kk}}\right)} \tag{3.6}$$

and

$$\epsilon_{jk} = \frac{\Delta A_{jk}\,\epsilon_{kk}}{\Delta A_{kk}} \tag{3.7}$$

Each ϵ_{jj} can be calculated after $\epsilon_{j-1,j-1}$ has been calculated. This indicates that ϵ_{11} on which all other ϵ's depend, should be measured as accurately as possible.

To calculate the temperature profile, the reversal temperature at various locations x are obtained. A plot would give a profile probably similar to the intensity profile. Let us now see what the reversal temperatures mean. At location x = 1, the radiation of the light source alone is, according to Wien's formula,

$$I_{S1} = C_1\lambda^{-5} e^{-C_2/\lambda T_{S1}} \tag{3.8}$$

where the subscripts S and 1 in I_{S1} and T_{S1} denote light source and location 1 respectively, C_1, C_2 are the radiation constants, and T_{S1} = brightness temperature of the source image at the flame. [C_2 = 1.4387 cm-°K, so that if λT is < .31, Wien's formula introduces an error of less than 1% over the correct Planck's formula. At the D-line wavelength, this means T should be < 5270°K for Wien's formula to be correct within the 1% error.] The radiation intensity of the light source plus the flame can be written as:

$$I_{(S+f)1} = C_1\lambda^{-5} e^{-C_2/\lambda T_{S1}}(1 - \epsilon_{11})^2 + C_1\lambda^{-5} e^{-C_2/\lambda T_{11}}[\epsilon_{11} + \epsilon_{11}(1 - \epsilon_{11})] \tag{3.9}$$

where the first term on the right hand side of the equation represents the light source radiation as transmitted through the flame and the second term represents radiation of flame from the two elemental areas denoted by ΔA_{11}. At reversal $I_{S1} = I_{(S+f)1}$ and therefore combining Eqs. (3.8) and (3.9) and dividing through by $C_1\lambda^{-5}$, we obtain:

$$e^{-C_2/\lambda T_{S1}}\left[1 - (1 - \epsilon_{11})^2\right] = e^{-C_2/\lambda T_{11}}(2\epsilon_{11} - \epsilon_{11}^2) \tag{3.10}$$

so that

$$T_{S1} = T_{11} = T_{j1}, \tag{3.11}$$

since axisymmetry is assumed.

At location x = 2, the radiation intensity of the source alone is

$$I_{S2} = C_1\lambda^{-5} e^{-C_2/\lambda T_{S2}} \tag{3.12}$$

and that of the source and the flame simultaneously is

$$\begin{aligned} I_{(S+f)2} = {} & C_1\lambda^{-5} e^{-C_2/\lambda T_{S2}} (1 - \epsilon_{21})^2(1 - \epsilon_{22})^2 \\ & + C_1\lambda^{-5} e^{-C_2/\lambda T_{11}} \epsilon_{21}[(1 - \epsilon_{22})^2(1 - \epsilon_{21}) + 1] \\ & + C_1\lambda^{-5} e^{-C_2/\lambda T_{22}} \epsilon_{22}[(1 - \epsilon_{22})(1 - \epsilon_{21}) + (1 - \epsilon_{21})] \end{aligned} \tag{3.13}$$

Again at reversal Eqs. (3.12) and (3.13) are equal, therefore

$$\begin{aligned} e^{-C_2/\lambda T_{S2}}[1 - (1 - \epsilon_{21})^2(1 - \epsilon_{22})^2] = {} & e^{-C_2/\lambda T_{11}}[(1 - \epsilon_{22})^2(1 - \epsilon_{21}) + 1]\epsilon_{21} \\ & + e^{-C_2/\lambda T_{22}}(1 - \epsilon_{21})[(1 - \epsilon_{22}) + 1]\epsilon_{22} \end{aligned} \tag{3.14}$$

Now T_{11} has been previously found to be equal to T_{S1}. If T_{S2} happens to be equal to T_{S1}, then it can be verified after expanding Eq. (3.14) that $T_{22} = T_{S1}$. This indicates that if the reversal temperature distribution is uniform, the temperature of the flame is uniform also and is correctly given by the reversal temperature. Furthermore this result is independent of the emissivity distribution of the flame so that this distribution need not be calculated.

In general, the reversal temperature distribution may not be uniform and therefore the temperature profile has to be calculated step by step as outlined above. As an aid in this calculation, the general reversal equation is given here:

$$e^{-C_2/\lambda T_{Sj}} \left[1 - \prod_{k=1}^{k=j} (1 - \epsilon_{jk})^2 \right] =$$

$$\sum_{n=1}^{j} e^{-C_2/\lambda T_{nn}} \epsilon_{jn} \left[\frac{\prod_{k=1}^{j} (1 - \epsilon_{jk})^2}{\prod_{n=1}^{j} (1 - \epsilon_{jn})} + \prod_{n=1}^{j} (1 - \epsilon_{j,n-1}) \right] \qquad (15)$$

The last term of the summation series would be a function of T_{jj}, whereas all the other terms of the equation are either known or have been calculated in the previous steps. Thus the actual radial temperature profile of the flame can be found.

IV. IGNITION TIME DELAY

INTRODUCTION

The results of experiments on standing detonation waves with hydrogen-air mixtures at The University of Michigan have consistently revealed a distinct separation between the shock wave and flame front. This separation corresponds to the ignition time delay. In view of these results, it appeared essential and opportune to consider this facet theoretically and attempt to corroborate the experimental observations. Such knowledge is of great value to the understanding of the structure of a detonation wave. In addition, it is well to assess the potential value of this steady flow experimental technique to the study of chemical kinetics. Accordingly, a theoretical and experimental investigation of the ignition time delay of hydrogen-oxygen mixtures under detonation or near detonation conditions was effected.

This problem has been treated in detail by Nicholls and was reported in an earlier report on this project. Subsequent work has led to a more rigorous treatment of the pertinent reaction equations so that it is deemed appropriate to include the results herein.

The problem to be considered is that wherein a hydrogen-oxygen-diluent mixture is subjected to a normal shock wave sufficiently strong to cause ignition. It is known (Semenov[8] and Lewis and von Elbe[4]) that under these conditions an induction period must exist before any explosion can materialize. Duff[9] clarified the problem by calculating numerically the reaction profile of a $2H_2+O_2+X_e$ mixture behind a steady state shock wave for a given Mach

number, temperature, and pressure. His results for the particular conditions considered indicated that the well-known hydrogen-oxygen chain branching mechanism was established almost immediately. Thus, theinduction period in the case of high temperatures represents the time required by the action of the chain to establish radical concentrations and hence rates of reaction that are great enough to affect the thermodynamic and hydrodynamic variables. Once this condition is attained, the temperature rises rapidly and the flame is established. Schott and Kinsey[10] performed calculations similar to those of Duff and also measured the OH concentration in the shock wave induced reaction of argon diluted hydrogen-oxygen mixtures. They interpreted their ignition delay data in terms of the rate controlling reaction for the branched chain mechanism, the primary initiation reaction, and the time required for the OH concentration to attain a certain value. In this paper we treat Duff's comprehensive reaction scheme analytically with major emphasis placed on the time dependent description of the hydrogen atom concentration. A physically plausible condition is then invoked which allows prediction of the ignition delay time. The results of this analysis will be compared with the experimentally measured delays described in this paper.

The problem will be generalized to the extent of including reactions of the type:

$$xH_2 + yO_2 + zB \longrightarrow \text{products}$$

where B is some unspecified inert gas. Hence various hydrogen-oxygen concentrations as well as diluent concentrations will be considered. It will be assumed that no chemical reaction occurs across the shock wave and further

that the gases are immediately equilibrated in the rotational and translational degrees of freedom. Realizing that shock waves are only a few mean free paths in thickness, that only 3-5 and 15-300 molecular collisions are required to equilibrate the translational and rotational degrees respectively, and that many thousands of collisions are generally required to complete a chemical reaction, it would appear that the assumptions are perfectly justifiable. Supporting arguments for these conclusions are given by Bethe and Teller,[11] Wood,[12] and many others. The question of relative times for ignition delay and vibrational relaxation is not well established as has been discussed by Schott and Kinsey[10] and Patch.[13] Evidently there is the distinct possibility that for certain hydrogen-oxygen-nitrogen mixtures the vibrational relaxation time may be much shorter than, much greater than, or of the same order as the ignition time delay. In the following theoretical development it will be assumed that the vibrational relaxation time is either much shorter or much longer than the ignition time delay so that a temperature may be readily defined without ambiguity. It will not be necessary to assert which of the two cases prevails until one attempts to determine the temperature and pressure behind the shock in terms of the upstream conditions. This problem will arise in a later part of this paper when the experimental results are compared with theory. At that point it will be assumed that vibration is not excited behind the wave, that is, that the vibrational relaxation time is much longer than the ignition delay time.

Throughout the induction zone it is safe to assume no change in the total number of moles per cc (i.e., [C] = constant) inasmuch as the total number of

moles of radicals and H_2O formed is relatively small. Similarly, the mole fractions of H_2 and O_2 will remain almost constant although this condition will subsequently be relaxed in the late stages of the induction period. For the same reason (changes only on the microscopic level), the thermodynamic coordinates and hydrodynamic variables remain fixed so that it is possible to divorce the chemical kinetics from the fluid mechanics. This, of course, greatly simplifies the problem.

PERTINENT REACTIONS AND RATES OF REACTION

Some of the more important reactions characterizing the combustion of H_2-O_2 mixtures have been postulated by various authors (cf, Semenov[8] and Lewis and von Elbe[4]). There has not been complete agreement on all of these reactions. Duff[9] considered 9 reactions and calculated, by iterative techniques, the reaction profile behind a shock wave moving through a $2H_2+O_2+X_e$ mixture such that the pressure and temperature immediately downstream of the shock were 1.150 atmospheres and 1737°K respectively. For this purpose he utilized the best known values of the rate constants. Inasmuch as Duff's reaction scheme appears to be the most comprehensive and recent and is in the temperature range of interest here, his proposed reactions will be considered in this work. The aim will be to reduce the reaction scheme to a form that can be handled analytically so that functional information can be gained.

The reactions to be considered are given in Table I. The reactions, $H+O_2+M \rightarrow HO_2+M$ along with two other consequent reactions given by Patch,[13] are not included in that they would be of importance only for temperatures below about 1100°K. Consequently, the subsequent predictions of ignition time

delay can be expected to hold only for higher temperatures.

TABLE I

PERTINENT REACTIONS IN THE IGNITION DELAY ZONE

No.	Reaction
I	$H_2O + M \xrightarrow{k_1} OH + M + H$
II	$H_2 + M \xrightarrow{k_2} 2H + M$
III	$O_2 + M \xrightarrow{k_3} 2O + M$
IV	$OH + M \xrightarrow{k_4} O + H + M$
V	$O_2 + H_2 \xrightarrow{k_5} 2\ OH$
VI	$O_2 + H \xrightarrow{k_6} OH + O$
VII	$H_2 + O \xrightarrow{k_7} OH + H$
VIII	$H_2 + OH \xrightarrow{k_8} H_2O + H$
IX	$2\ OH \xrightarrow{k_9} H_2O + O$

(M = some third body)

The reactions have been written as proceeding only in the forward direction. This is legitimate for the induction period in that the gas immediately behind the shock is far removed from chemical equilibrium and hence the reverse reaction rates will be negligible. Of course, in the later stages as the reaction nears equilibrium the reverse rates will have to be taken into account. Fortunately, for the problem at hand, this added complexity will not arise.

The reaction rate constant, k_i (the subscript i referring to the particular reaction in Table I), is given by:

$$k_i = A_i T^{m_i} \exp(-\frac{E_i}{RT})$$

The values of A_i, m_i, and E_i, as given by Duff, are tabulated in Table II.

TABLE II

VALUES FOR THE REACTION RATE CONSTANT

Reaction No.	E(cal/mole)	m	$A\left(\frac{\text{moles}}{\text{cc}}\right)^{-1}\text{sec}^{-1}$
I	(a) 1.1473×10^5	-1.5	10^{21}
	(b) 1.1473×10^5	-1.5	10^{23}
II	1.0324×10^5	-1.5	10^{21}
III	1.1796×10^5	-1.5	10^{21}
IV	1.01×10^5	-1.5	10^{21}
V	7×10^4	0	10^{14}
VI	(a) 2.0×10^4	0	10^{14}
	(b) 1.8×10^4	0	4×10^{14}
VII	6×10^3	0	3×10^{14}
VIII	2.5×10^3	0	3×10^{14}
IX	2.5×10^3	0	3×10^{14}

Particular values for k_i at a few temperatures over the range of interest are presented in Table III.

In writing the individual rate equations, it is convenient to non-dimensionalize the species concentrations by writing $n_H = [H]/[C]$, $n_O = [O]/[C]$, etc. In comparing the importance of individual terms of the rate equations we note that n_{O_2} and n_{H_2} are of order unity, written as $O(n_{O_2}) = 1$ and $O(n_{H_2}) = 1$. The concentrations of all radicals are much less than that of H_2 and O_2 so that,

$$n_H \ll 1, \quad n_{H_2O} \ll 1, \quad n_{OH} \ll 1, \quad n_O \ll 1$$

TABLE III

REACTION RATE CONSTANT AT DIFFERENT TEMPERATURES

$k_i\left(\frac{\text{moles}}{\text{cc}}\right)^{-1}\text{sec}^{-1}$	1000°K	T°K 1500°K	2000°K
k_{1a}	2.51×10^{-9}	3.24×10^{-1}	3.31×10^{3}
k_{1b}	2.51×10^{-7}	3.24×10	3.31×10^{5}
k_2	7.97×10^{-7}	1.61×10	5.62×10^{4}
k_3	5.02×10^{-10}	1.05×10^{-1}	1.41×10^{3}
k_4	2.50×10^{-6}	3.24×10	1.00×10^{5}
k_5	5.02×10^{-2}	6.30×10^{3}	2.24×10^{6}
k_{6a}	4.26×10^{9}	1.02×10^{11}	6.53×10^{11}
k_{6b}	4.68×10^{10}	9.52×10^{11}	4.32×10^{12}
k_7	1.47×10^{13}	4.00×10^{13}	6.63×10^{13}
k_8	8.53×10^{13}	1.30×10^{14}	1.60×10^{14}
k_9	8.53×10^{13}	1.30×10^{14}	1.60×10^{14}

In veiw of these inequalities and the values of the rate constants given in Table III, it is possible to immediately eliminate some terms from the rate equations.

Defining the constants:

$$a = [C]\,k_1 \qquad f = n_{O_2}[C]k_6$$

$$b = 2n_{H_2}[C]k_2 \qquad g = n_{H_2}[C]k_7$$

$$c = 2n_{O_2}[C]k_3 \qquad h = n_{H_2}[C]k_8$$

$$\epsilon = 2n_{O_2}n_{H_2}[C]k_5 \qquad i = [C]k_9$$

the resultant rate equations may be written:

$$\frac{dn_H}{dt} = \dot{n}_H = b - fn_H + gn_O + hn_{OH} \tag{4.1}$$

$$\dot{n}_O = c + fn_H - gn_O + in_{OH}^2 \tag{4.2}$$

$$\dot{n}_{OH} = \epsilon + fn_H + gn_O - hn_{OH} \tag{4.3}$$

$$\dot{n}_{H_2O} = - an_{H_2O} + hn_{OH} \tag{4.4}$$

$$\dot{n}_{O_2} = - \frac{1}{2} \epsilon - fn_H \tag{4.5}$$

$$\dot{n}_{H_2} = - \frac{1}{2} \epsilon - gn_O - hn_{OH} \tag{4.6}$$

These equations are valid throughout the entire induction zone but at different times different terms predominate.

SOLUTION OF THE EQUATIONS

The nonlinear term of Eq. (4.2) may be dropped because at the initial stages of the ignition delay zone it is small compared to "c" and at the later stages it is small compared to fn_H and gn_O. This step will be discussed in a subsequent section.

The first 3 equations then become linear in the 3 unknowns $n_H(t)$, $n_O(t)$, and $n_{OH}(t)$ and hence can be readily solved. Introducing the linear transformations,

$$\xi = n_H - \delta_1$$

$$\eta = n_O - \delta_2$$

$$\zeta = n_{OH} - \delta_3$$

and choosing the constants conveniently as,

$$\delta_1 = - \frac{(\frac{b+\epsilon}{2} + c)}{f}$$

$$\delta_2 = -\frac{b + \epsilon}{2g}$$

$$\delta_3 = -\frac{b + c}{h}$$

the equations become;

$$\dot{\xi} = -f\xi + g\eta + h\zeta \tag{4.7}$$

$$\dot{\eta} = f\xi - g\eta \tag{4.8}$$

$$\dot{\zeta} = f\xi + g\eta - h\zeta \tag{4.9}$$

The solutions are:

$$\xi = \sum_{i=1}^{3} a_i e^{\lambda_i t}$$

$$\eta = \sum_{i=1}^{3} a_i b_i e^{\lambda_i t}$$

$$\zeta = \sum_{i=1}^{3} a_i c_i e^{\lambda_i t} \tag{4.10}$$

The quantities λ_i, b_i, and c_i may be expressed in terms of the a_i by substitution of relations (4.10) into (4.7), (4.8), and (4.9). Then the a_i's are evaluated from the boundary conditions, i.e., at

$$t = 0, \quad n_H = n_O = n_{HO} = 0$$

The results, after dropping the insignificant terms, are:

$$\lambda_1 = 2f \qquad \lambda_2 = -h \qquad \lambda_3 = -g$$

$$a_1 = \frac{b + \epsilon}{2f} \qquad a_2 = \frac{\epsilon}{h} \qquad a_3 = \frac{\epsilon f}{g} \frac{(g - 2h)}{(h - g)^2}$$

$$b_1 = \frac{f}{g} \qquad b_2 = \frac{f}{g - h} \qquad b_3 = \frac{g - h}{g - 2h}$$

$$c_1 = \frac{2f}{h} \qquad c_2 = -1 \qquad c_3 = \frac{g}{g - 2h}$$

In arriving at these forms the inequalities $f \ll h$ and $g \simeq h$ but $g \neq h$ were used. These inequalities are good for the values of reaction rate constants used and as long as the order of magnitude of n_{O_2} and n_{H_2} is the same.

The resultant expressions for the concentrations of radicals for all t, neglecting the very small terms, are:

$$n_H(t) = \frac{b + \epsilon}{2f} (e^{2ft} - 1) + \frac{\epsilon}{h} e^{-ht} \tag{4.11}$$

$$n_O(t) = \frac{b + \epsilon}{2g} (e^{2ft} - 1) - \frac{\epsilon f}{h(h - g)} e^{-ht} + \frac{\epsilon f}{g(h - g)} e^{-gt} \tag{4.12}$$

$$n_{OH}(t) = -\frac{b + c}{h} + \frac{b + \epsilon}{h} e^{2ft} - \frac{\epsilon}{h} e^{-ht} + \frac{\epsilon f}{(h - g)^2} e^{-gt} \tag{4.13}$$

$$n_{H_2O}(t) = \frac{b + \epsilon}{2f} (e^{2ft} - 1) + \frac{\epsilon}{h} e^{-ht} = n_H \tag{4.14}$$

It is convenient at this point to introduce a characteristic time, $t_c = 1/h = 1/n_{H_2}[C]k_8$, which is based on the initial hydrogen mole fraction, the total concentration, and the fastest reaction rate constant. Also define a dimensionless time,

$$t' = \frac{t}{t_c} = ht$$

The characteristic time is much less than the ignition time delay so it is in order to rewrite Eqs. (4.11-4.14) for $t' \gg 1$. They are:

$$n_H(t) = \frac{b + \epsilon}{2f} (e^{2ft} - 1) \tag{4.15}$$

$$n_O(t) = \frac{b + \epsilon}{2g} (e^{2ft} - 1) = \frac{f}{g} n_H \tag{4.16}$$

$$n_{OH}(t) = \frac{b + \epsilon}{h} e^{2ft} = \frac{2f}{h} n_H + \frac{b + \epsilon}{h} \tag{4.17}$$

$$n_{H_2O}(t) = \frac{b + \epsilon}{2f}(e^{2ft} - 1) = n_H \tag{4.18}$$

It is evident from these equations that for the time periods of interest ($t' \gg 1$) the H_2O concentration will be identical with that of H, the O concentration will be a very small constant fraction of the H concentration and the OH concentration will be approximately the same as that of O. The form of these equations is, of course, directly attributable to the action of the chain; reactions VI, VII, and VIII. The equality of n_H and n_{H_2O} is a consequence of the fastest reaction (VIII) which produces H_2O at the same rate as H.

Equations (4.11-4.18) are plotted in Fig. 4 for a temperature of 1500°K and for a stoichiometric mixture of hydrogen-oxygen. It is evident from the merging of the two forms of each radical equation that the action of the chain becomes a dominating factor before 10 t'. Thus the characteristic time has the physical significance of being a transition time between the important initiation reactions and the action of the chain.

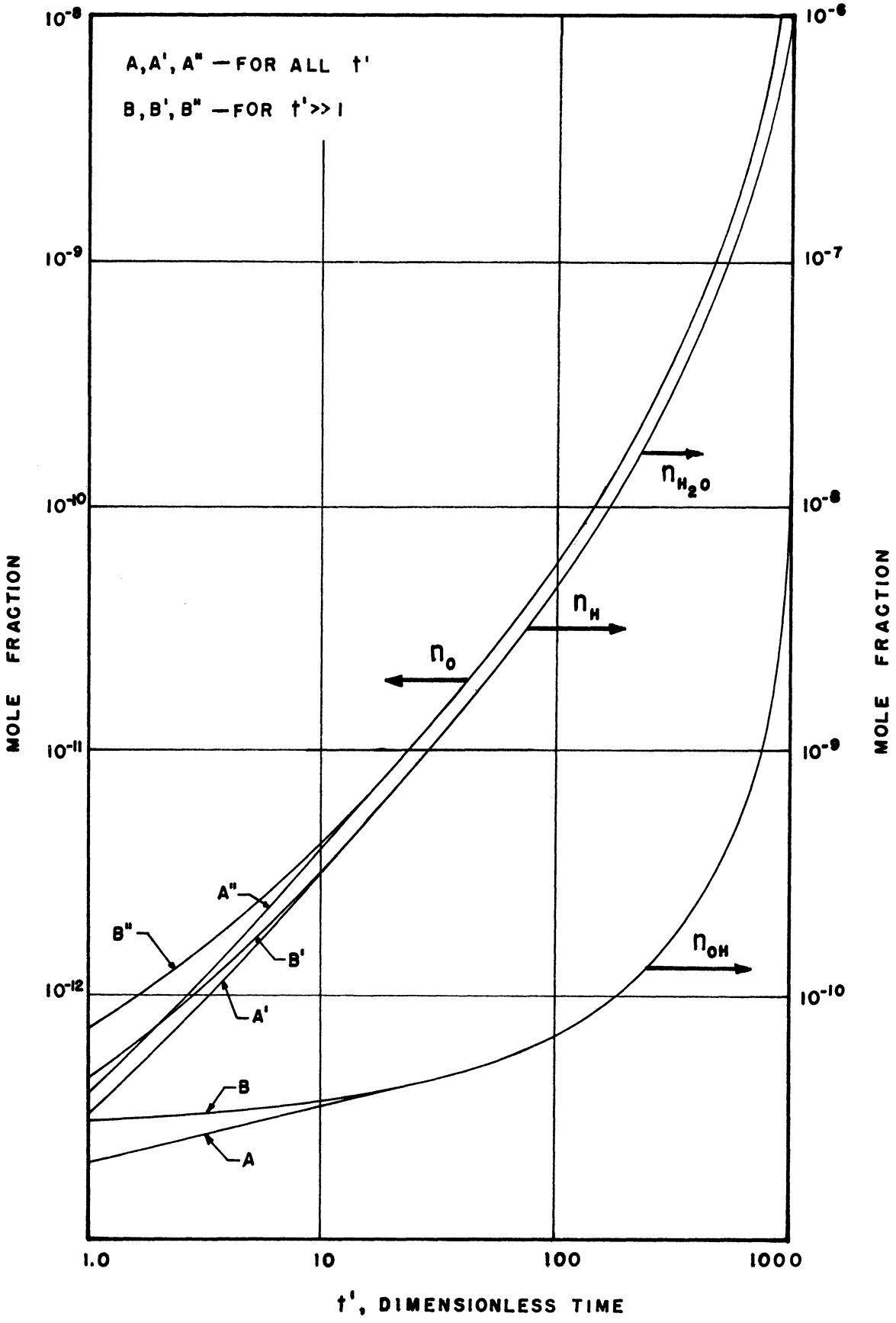

Fig. 4. Radical concentration during the ignition delay period.

IGNITION TIME DELAY

It is now pertinent to define a time, τ, which is representative of the ignition delay. Once a sufficient number of hydrogen atoms have been produced (late in the induction period), the various reactions occur rapidly and exothermally to the degree that the temperature begins to increase. This increases the reaction rate exponentially so that the temperature soon increases exponentially. The "flame" is established shortly thereafter. It would appear logical, then, to define τ as the time required for n_H to attain some suitably high value, λ. The expression for ignition time delay can then be written directly from Eq. (4.15). That is,

$$\tau = \frac{1}{2f} \ell n \left(\frac{2f}{b + \epsilon} \lambda + 1 \right) \tag{4.19}$$

Many equally valid criteria may be proposed for ascertaining λ, all of which lead to essentially the same value of τ. However it would appear consistent to arrive at a criteria based on the rate controlling reaction, $H+O_2 \xrightarrow{k_6} OH+O$, wherein account is taken of the decreasing oxygen concentration. Noting that $(b+\epsilon)2f$ is at most of the order of 10^{-6} in Eq. (4.15) and that λ must be orders higher allows (4.15) to be written:

$$n_H(t) = \frac{b + \epsilon}{2f} e^{2ft}$$

so that,

$$\dot{n}_H = (b + \epsilon) e^{2ft} = 2fn_H = 2n_{O_2} n_H [C] k_6 \tag{4.20}$$

In the very late stages of the delay zone n_{O_2} decreases in accordance with Eq. (4.8) which, after dropping the small term, is:

$$\dot{n}_{O_2} = - fn_H = - \frac{1}{2} \dot{n}_H$$

This integrates to,

$$n_{O_2} - (n_{O_2})_0 = - \frac{1}{2} n_H \qquad (4.21)$$

where now n_{O_2} is taken as time dependent and $(n_{O_2})_0$ is the initial value of n_{O_2}. Differentiating (4.20) and substituting (4.21) yields,

$$\ddot{n}_H = 2(n_{O_2})_0 \dot{n}_H[C]k_6 - 2n_H \dot{n}_H[C]k_6$$

Let us now arbitrarily say that λ will be that value of n_H corresponding to the inflection point in the n_H versus t curve; that is, where n_H is a maximum and $\ddot{n}_H$ is 0. Thus,

$$(n_H)_\tau = \lambda = (n_{O_2})_0$$

This λ then defines a time representative of the ignition delay in a manner independent of the particular initial concentrations employed. As seen, the actual value of λ is based on an initial concentration.

Substituting for λ in (4.19) and noting that $\frac{2f}{\epsilon} n_{O_2} \gg 1$, we have,

$$\tau = \frac{1}{2f} \ell n \frac{(2fn_{O_2})}{b + \epsilon} = \frac{1}{2n_{O_2}[C]k_6} \ell n \left[\frac{n_{O_2}^2 k_6}{n_{H_2} k_2 + n_{H_2} n_{O_2} k_5} \right] \qquad (4.22)$$

where the subscript on n_{O_2} has been dropped but it is to be understood that it represents the initial mole fraction. The logarithm term in (4.22) has slight but not negligible influence on τ. Thus we see that the ignition time delay is dependent almost solely on the action of the chain. That is, the

time required for the initiation processes to start the chain is negligible.

We can rewrite the equation, noting that [C] = P/RT, as

$$\tau = \frac{RT}{2n_{O_2}PA_6} e^{E_6/RT} \ln \left[\frac{n_{O_2}^2 k_6}{n_{H_2}k_2 + n_{H_2}n_{O_2}k_5} \right] \qquad (4.23)$$

The following conclusions can be drawn:

(a) $\ln\tau$ is only approximately proportional to reciprocal temperature wherein the slope is indicative of the activation energy of the controlling reaction.

(b) τ is inversely proportional to pressure.

(c) τ is approximately inversely proportional to the initial mole fraction of oxygen.

(d) τ is weakly sensitive to n_{H_2}.

(e) τ is independent of the particular inert gas, being dependent only on the mole fraction of inert present.

Equation (4.22) is plotted in Fig. 5 for both a stoichiometric hydrogen-oxygen and stoichiometric hydrogen-air mixture at one atmosphere. The values of k_6 were taken as those corresponding to k_{6b} in Table II. A curve is also included for the hydrogen-oxygen mixture with $k_6 = k_{6a}$. As can be seen, the hydrogen-oxygen mixtures involve shorter time delays for the same value of the rate constant. This is almost entirely due to the difference in n_{O_2}, the value of n_{H_2} having only secondary effect.

The assumption was made throughout most of the analysis that n_{O_2} could be taken as a constant. The validity of this assumption insofar as it affects the prediction of ignition time delay can be justified through use of

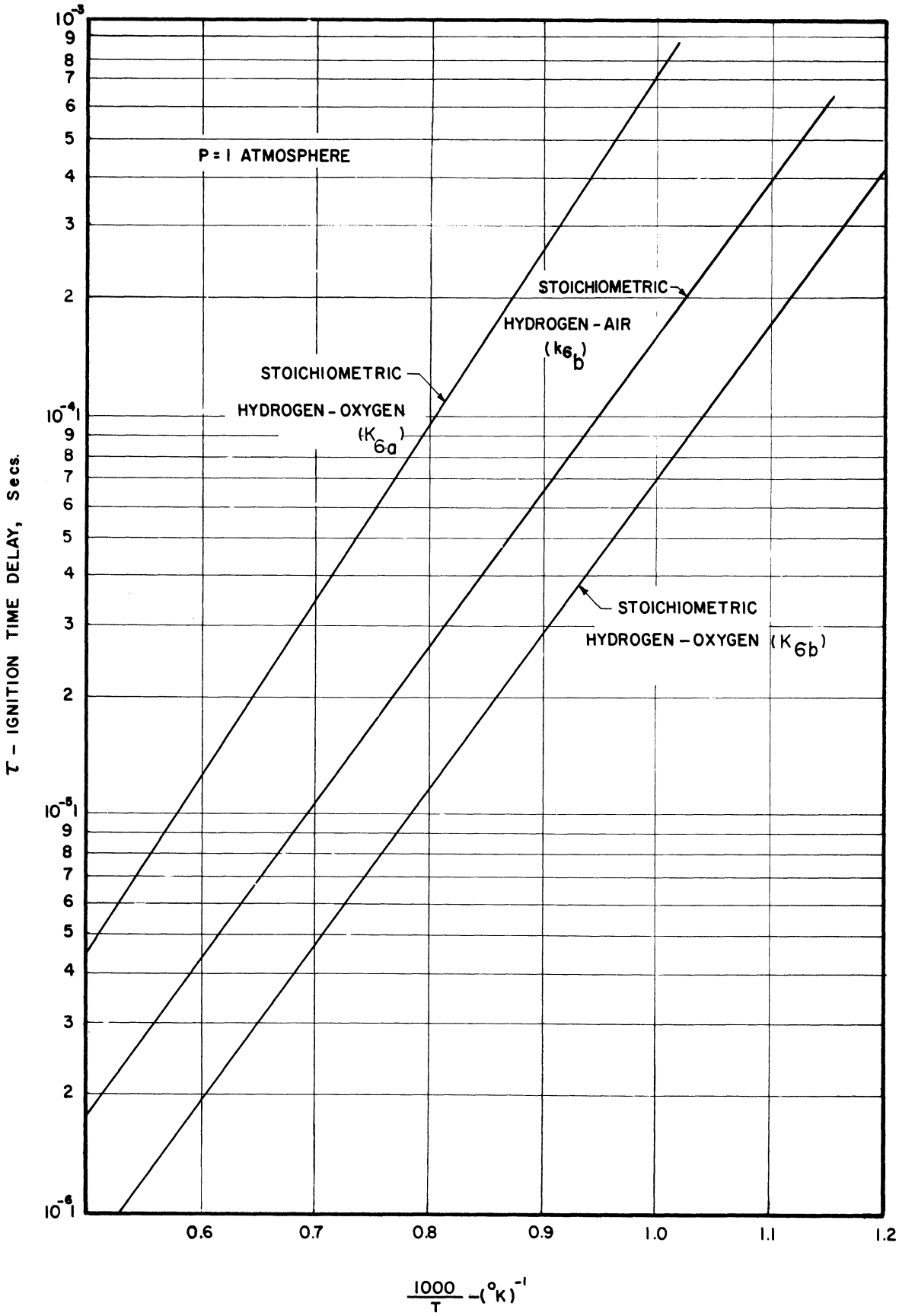

Fig. 5. Ignition time delay for H_2-O_2 and H_2-air mixtures at different temperatures.

Eqs. (4.15) and (4.21) and the ignition delay criteria. A similar statement can be made and proven for the constancy of n_{H_2}.

COMPARISON BETWEEN THEORETICAL AND EXPERIMENTAL IGNITION DELAYS

Many experiments were conducted in the manner described in Section II wherein the hydrogen and air inlet conditions to the nozzle were varied. A typical simultaneous schlieren and direct photograph of the shock flame configuration is shown in Fig. 6. The flow is directed upwards and a portion of the nozzle can be seen in the lower part of the picture. The well defined delay zone is apparent.

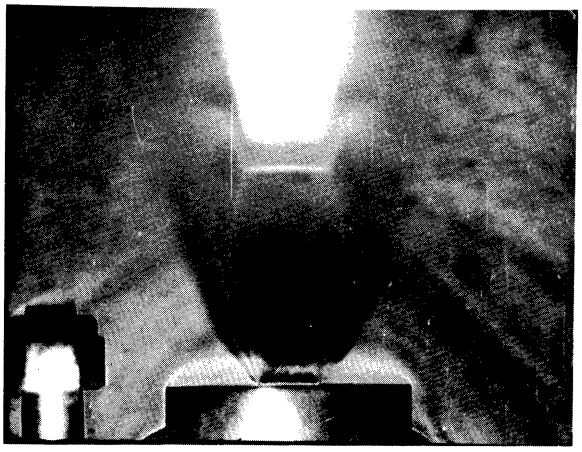

Fig. 6. Typical schlieren and direct photograph of a standing detonation wave (flame rendered visible by Na).

The jet calibration previously obtained allowed for the determination of all pertinent quantities behind the shock for the various runs. The delay distance, measured from the photographs as the distance from the shock to the visible "flame front," was then reduced to ignition delay time. Inasmuch as each of these runs were at varying fuel-air ratio and since the predominant effect of fuel-air ratio arises from the initial oxygen concentration, it is well

to consider $n_{O_2}[C]_\tau = [O_2]_\tau$ vs. $1/T$. The results are shown in Fig. 7 along with a plot of Eq. (4.22) where $k_6 = k_{6b}$. The experimental values are all seen to be smaller than the theoretical prediction, although this is subject to some reservation. The small scale of the experiment precluded accurate temperature measurements behind the shock so that it was necessary to ascertain this temperature indirectly from nozzle measurements and a previously determined calibration procedure. As a consequence, the temperature indicated could be in error by 40-50°K.

Probably the greatest source of scatter in the data arises from the complicated flow field downstream of the shock as described earlier. If one considers only the highest temperature runs, the agreement with theory is seen to be good and there is a minimum of scatter. Hence in those cases where the flame front is not too far from the shock (higher temperature operation), the assumption of a one dimensional flow in a constant area stream tube will be quite valid. At lower temperatures the induction zone will be subject to two dimensional fluid dynamic effects and the results thus invalidated. This facet is elaborated upon in Section VI.

This fact introduces an aerodynamic limitation on the range of conditions that may be investigated with this experimental technique in the scale of the experiment utilized. Longer delay times may be studied by enlarging the jet structure. This may be accomplished by using a larger nozzle with a consequent increase in the gaseous flow rates, by operating at higher pressure, or by discharging into sub-atmospheric pressure.

The prediction of values of activation energy and frequency factor would

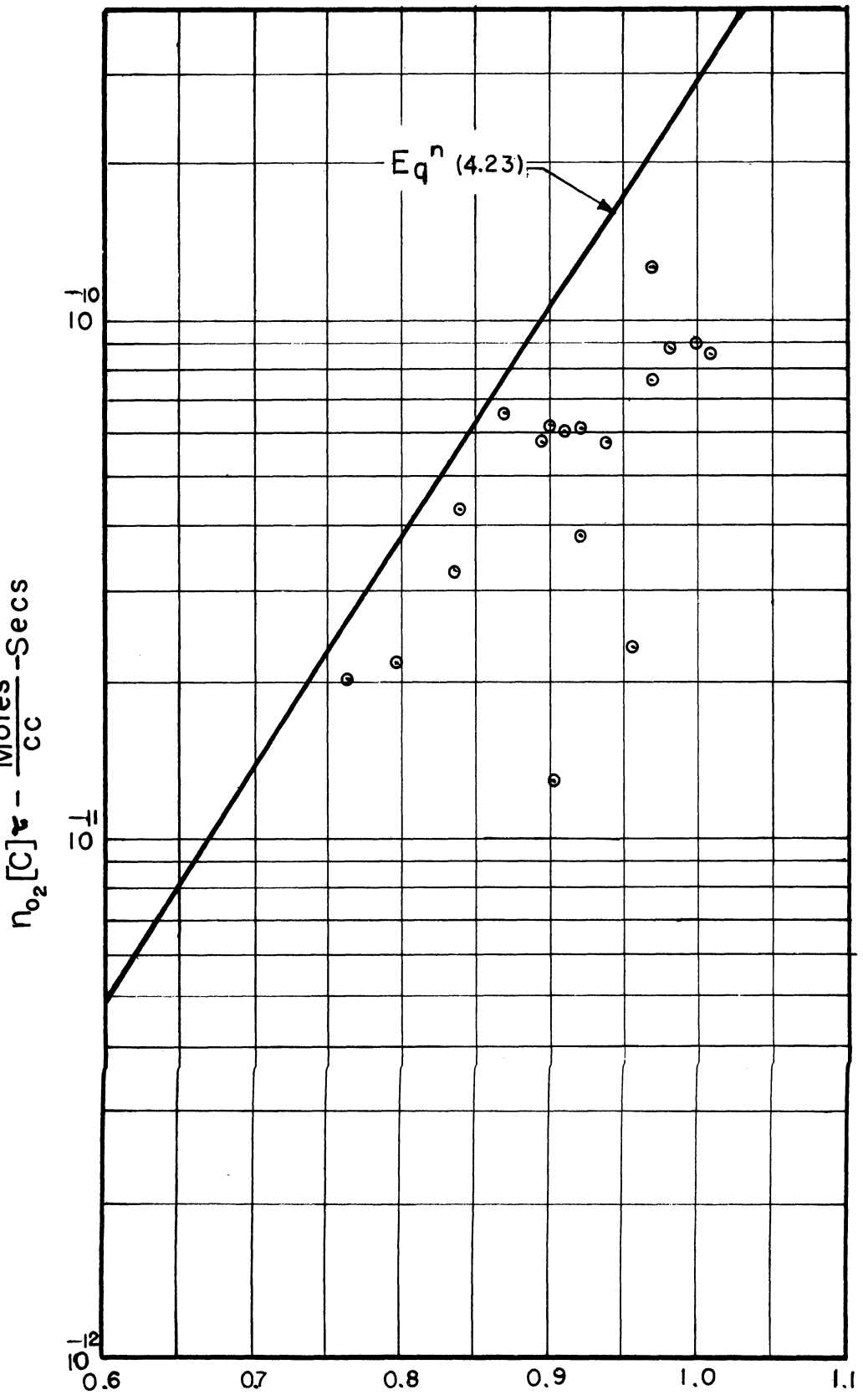

Fig. 7. Comparison of theoretical and experimental time delays for H_2-air.

be one of the aims of experiments of this type. At the present time, however, more accurate measurements are required. Preferably this means that temperatures, pressures, and composition measurements should be effected under actual run conditions in order to forego the use of calibration procedures which do not cover the entire range of operation. For such measurements water cooled probes would undoubtedly be required which are too large for the present small scale experiments. It is felt that the agreement of experiment with theory as reported here is very satisfactory and that it has been proven that this experimental technique, with some refinements, has great application to the study of chemical kinetics.

Other results on induction times in the hydrogen-oxygen reaction have been reported by Schott and Kinsey.[10] Their results were compared to the results of this paper in a previous publication and hence shall not be discussed further here.

Patch[13] has considered the kinetics of the hydrogen-oxygen-diluent system with special application to the prediction of composition limits. The lower temperatures encountered necessitated the inclusion of some reactions which were not important in the temperature range of interest in this study (1100-2000°K). Conversely he did not include many of the reactions considered in this paper. If one neglects the dissociation of hydrogen and the reactions involving HO_2, Patch's prediction of the rate of growth of H is identical to that found in this paper for times much greater than the characteristic time.

V. VIBRATIONAL RELAXATION EFFECTS

Calculations are made to determine the gas temperatures behind strong shock waves produced in 10%, 20%, 30%, and 40% hydrogen-air mixtures so that the effects of vibrational relaxation on ignition time delay can be quantitatively assessed. The effects due to dissociation are not included in calculating this temperature. A steady, one-dimensional discontinuity is assumed. The model shown schematically below is adopted.

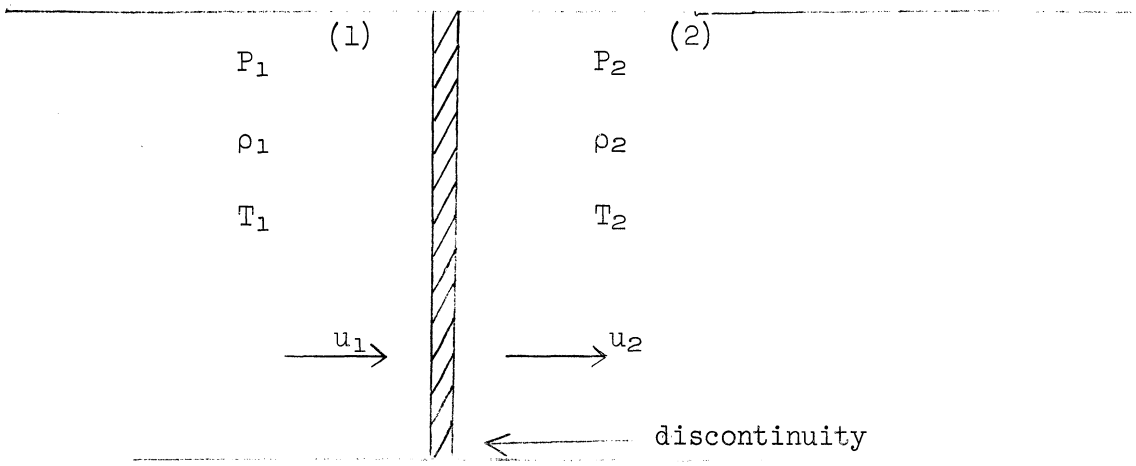

The Appropriate Flow Equations

Mass
$$\rho_1 u_1 = \rho_2 u_2 \tag{5.1}$$

Momentum
$$P_1 + \rho_1 u_1^2 = P_2 + \rho_2 u_2^2 \tag{5.2}$$

Energy
$$h_1 + \frac{u_1^2}{2} = h_2 + \frac{u_2^2}{2} \tag{5.3}$$

Algebraic Manipulation of the Flow Equations

The perfect gas assumption is made and the flow equations are manipulated to yield the following relations connecting the flow properties at state (1) and at state (2).

$$\frac{P_2}{P_1} = (F\gamma_1 M_1^2 + 1) \tag{5.4}$$

$$\frac{\rho_2}{\rho_1} = \frac{1}{(1 - F)} \tag{5.5}$$

$$\frac{T_2}{T_1} = (1 - F)(F\gamma_1 M_1^2 + 1) \tag{5.6}$$

where

$$F \equiv \left[1 - \left\{(1 + \delta) - \frac{h_2}{u_1^2/2}\right\}\right] \tag{5.7}$$

and

$$\delta = \frac{h_1}{u_1^2/2} \tag{5.8}$$

The F number defined herein is a somewhat generalized form of that introduced by Adamson and Morrison.[14] The onset of vibration, dissociation, combustion, etc., lead to different values of F and hence different values of all variables behind the wave. Hayes and Probstein[15] present a similar analysis wherein they define an

$$\epsilon \equiv \rho_1/\rho_2$$

which is related to F by

$$F = 1 - \epsilon.$$

The Chemical Equation

$$\alpha H_2 + O_2 + 3.76\ N_2 \longrightarrow$$

Total number of moles of mixture is: $4.76 + \alpha$ or, $M_T = 4.76 + \alpha$

for $\alpha = .10\ M_T$, $\alpha = .529$ moles of H_2

$\alpha = .20\ M_T$, $\alpha = 1.19$ moles of H_2

$\alpha = .30\ M_T$, $\alpha = 2.04$ moles of H_2

$\alpha = .40\ M_T$, $\alpha = 3.17$ moles of H_2

Molecular Weight of Mixture

α moles of H_2 x 2 $\frac{\text{gms}}{\text{mole}}$ $\quad 2\alpha$ gms

1 mole of O_2 x 32 $\frac{\text{gms}}{\text{mole}}$ $\quad 32$ gms

3.76 moles of N_2 x 28.02 $\frac{\text{gms}}{\text{mole}}$ $\quad 106$ gms

total gms of mixture $= (2\alpha + 138)$ gms

$$\therefore \text{ molecular weight of mixture } = \frac{2\alpha + 138}{\alpha + 4.76}$$

The Calculation Procedure

The calculation procedure is an iterative one. A value of α (hydrogen concentration) is chosen and a T_2 is assumed. The method then is to use this information to determine the corresponding enthalpy at state (2) from the following expression.

$$h_2 = \frac{RT_o}{(2\alpha + 138)} \left\{ [h]_{O_2} + 3.76\ [h]_{N_2} + \alpha [h]_{H_2} \right\} \frac{\text{cal}}{\text{gm of mix}}$$

where

$$R = 1.987\ \frac{\text{cal}}{\text{mole-}^\circ\text{K}}$$

$$T_o = 273^\circ\text{K}$$

and

[h] = the non-dimensional enthalpy obtained from the NBS circular No. 564 at the temperature, T_2.

The value of the enthalpy function thus calculated along with specified values of u_1 and δ is used in Eq. (5.7) to determine F. The F number is then employed to calculate T_2. This calculated T_2 is then compared with the assumed one and the whole procedure repeated a number of times until T_2(assumed) = T_2 (calculated).

An Alternate Method of Calculation

Another method which could be used to find the desired temperature without resorting to tabulated data is to express the enthalpy of the individual species as a function of temperature. The enthalpy of species k (assumed to be a perfect gas) can be written:

$$h_k = \Delta h^\circ_{fk} + \int_{T^\circ}^{T} C_{P_k} dT \quad \frac{\text{cal}}{\text{mole of k}}$$

Hence for a mixture of perfect gases at temperature, T_2

$$h_2 = \frac{1}{\sum_k \beta_k M_k} \left[\sum_k \beta_k \left(\Delta h^\circ_{fk} + R \int_{T^\circ}^{T_2} \frac{C_{P_k}}{R} dT \right) \right] \frac{\text{cal}}{\text{gm of mixture}}$$

where

β_k = number of moles of k^{th} gas in the mixture

M_k = molecular weight of k

Δh°_{fk} = heat of formation of k at $T^\circ = 0$

R = universal gas constant

C_{P_k} = specific heat at constant pressure of species k.

Now for a diatomic gas in the range of temperatures between the dissociation region and the region where van der Waals effects are important we can write after[16]

$$\frac{C_{P_k}}{R} = 3.5 + \left[\frac{\Theta_{v_k}/2T}{\sinh\left(\frac{\Theta_{v_k}}{2T}\right)}\right]^2$$

where Θ_{v_k} = characteristic vibrational temperature of the k^{th} gas.

for oxygen, $\Theta_v = 2275°K$

for nitrogen, $\Theta_v = 3398°K$

for hydrogen, $\Theta_v = 6328°K$

Substitution of this relation into the expression for h_2 and specialization to the case of hydrogen-air mixtures yields

$$h_2 = \frac{1}{2\alpha + 138}\left\{[h]_{O_2} + 3.76\,[h]_{N_2} + \alpha[h]_{H_2}\right\} \frac{cal}{gm \text{ of mixture}}$$

where

$$[h]_k = \left[3.5\,RT_2 + \frac{R\Theta_{v_k}}{\exp\left(\frac{\Theta_{v_k}}{T_2}\right) - 1}\right]_k \frac{cal}{mole}$$

Evaluation of h_2 by this method has given excellent agreement with the results using tabulated enthalpy data.

Graphic Presentation of $T_{2_{real}}$, $T_{2_{ideal}}$, $\frac{P_{2_{real}}}{P_{2_{ideal}}}$, and $\frac{\rho_{2_{real}}}{\rho_{2_{ideal}}}$ versus u_1 with α as parameter

The variation of $T_{2_{real}}$ and $T_{2_{ideal}}$ versus the velocity of the incident flow, u_1, is plotted in Fig. 8 for 10%, 20%, 30%, and 40% hydrogen-air mixtures. The corresponding variations of $\rho_{2_{real}}/\rho_{2_{ideal}}$ and $P_{2_{real}}/P_{2_{ideal}}$ are

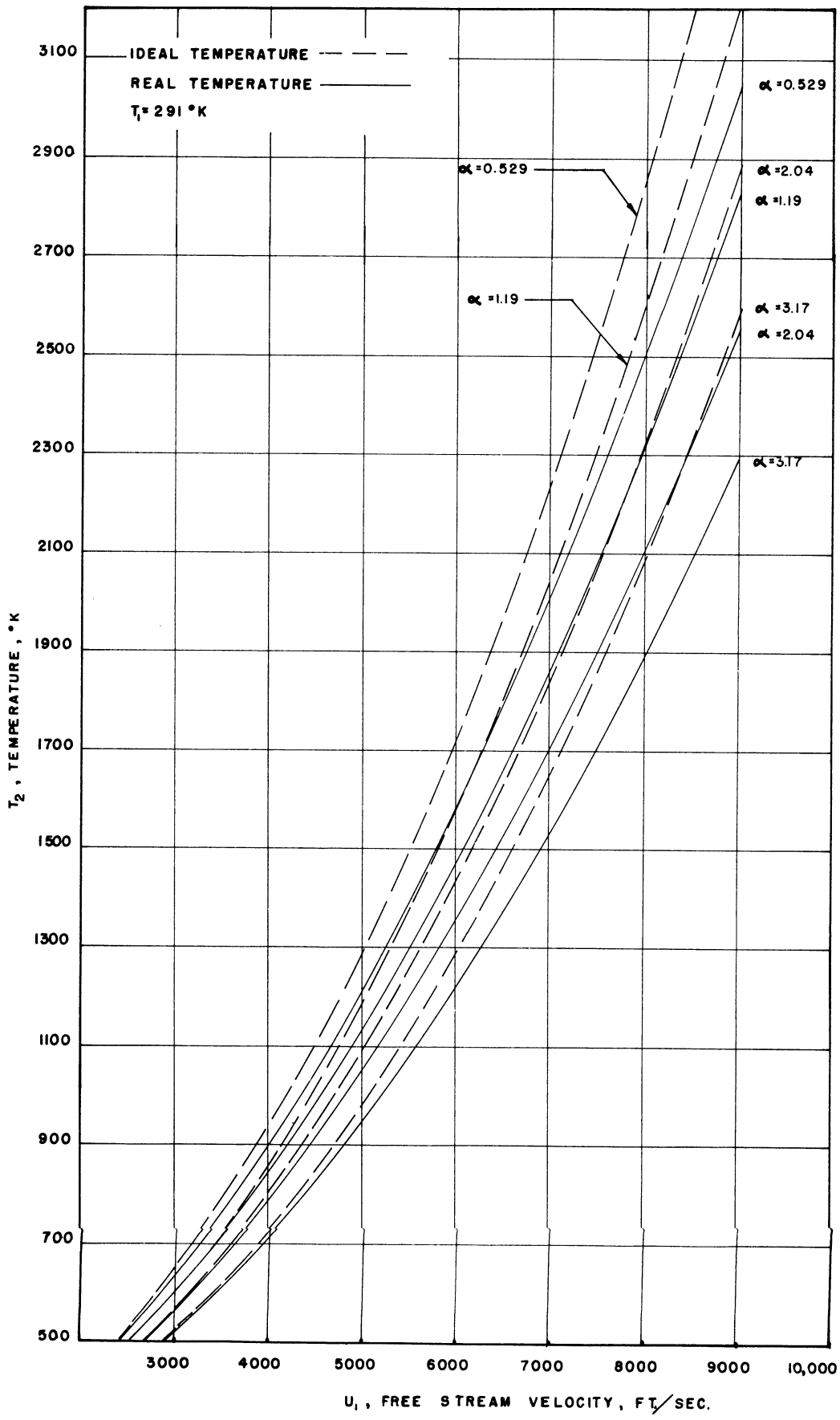

Fig. 8. Variation of real and ideal temperatures behind normal shocks with free stream velocity.

plotted in Fig. 9. The subscript "real" implies a consideration of vibrational relaxation but not dissociation. The ideal case is the one corresponding to constant specific heats.

It is seen that the differences between $T_{2_{ideal}}$ and $T_{2_{real}}$, $\rho_{2_{ideal}}$ and $\rho_{2_{real}}$, $P_{2_{ideal}}$ and $P_{2_{real}}$, at a given u_1 are larger for the hydrogen lean mixtures (e.g., α = .529 moles of H_2/mole mix) than they are for the hydrogen-rich mixtures (e.g., α = 3.17). The lean mixtures are subject to greater vibrational effects at a given temperature than are the rich mixtures at the same temperature in view of the high Θ_V for hydrogen. Hence, a greater proportion of the sensible thermal energy of the lean mixtures is transformed into internal energy of vibration resulting in a lower kinetic temperature, in a higher density, and in a higher pressure.

Application to the Prediction of Ignition Time Delay

In Section IV Eq. (4.23) was derived predicting the ignition time delay in hydrogen-air mixtures, this delay being extremely sensitive to temperature. As a consequence it can be expected that in those cases wherein the vibrational relaxation time, ν, is much smaller than the ignition time delay, τ, the delay time will be longer than when $\nu \gg \tau$. In order to assess this effect, the results of the preceding analysis are combined with the ignition delay analysis to arrive at the time differences to be expected. Considering a 20% (by volume) hydrogen-air mixture with the incoming conditions to the wave being T_1 = 291°K and the velocity, u_1, a variable, the calculated results for the two cases, $\nu \gg \tau$ and $\nu \ll \tau$, are as shown in Fig. 10. It is

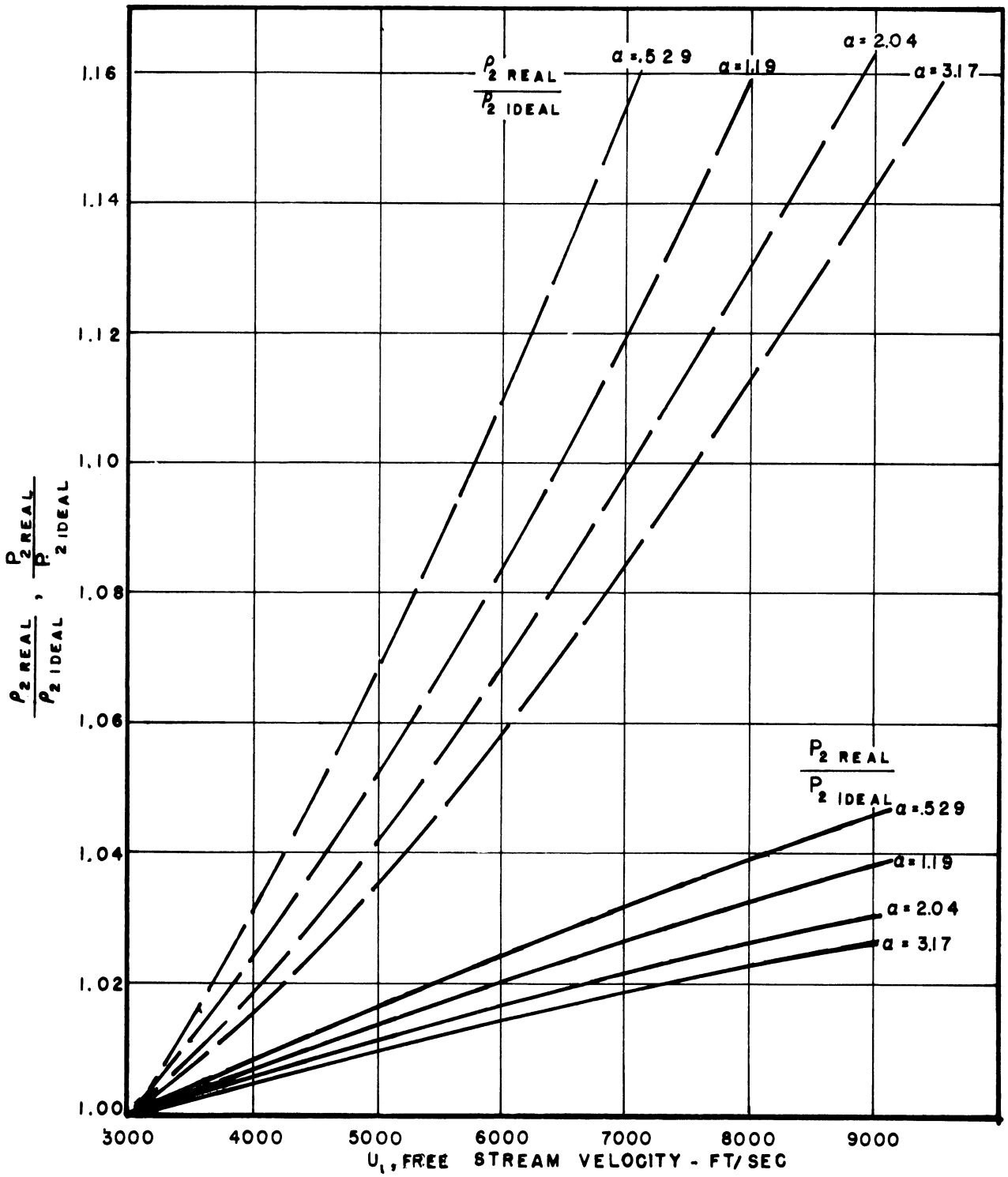

Fig. 9. Variation of $\rho_{2_{real}}/\rho_{2_{ideal}}$ and $P_{2_{real}}/P_{2_{ideal}}$ behind normal shocks with free stream velocity.

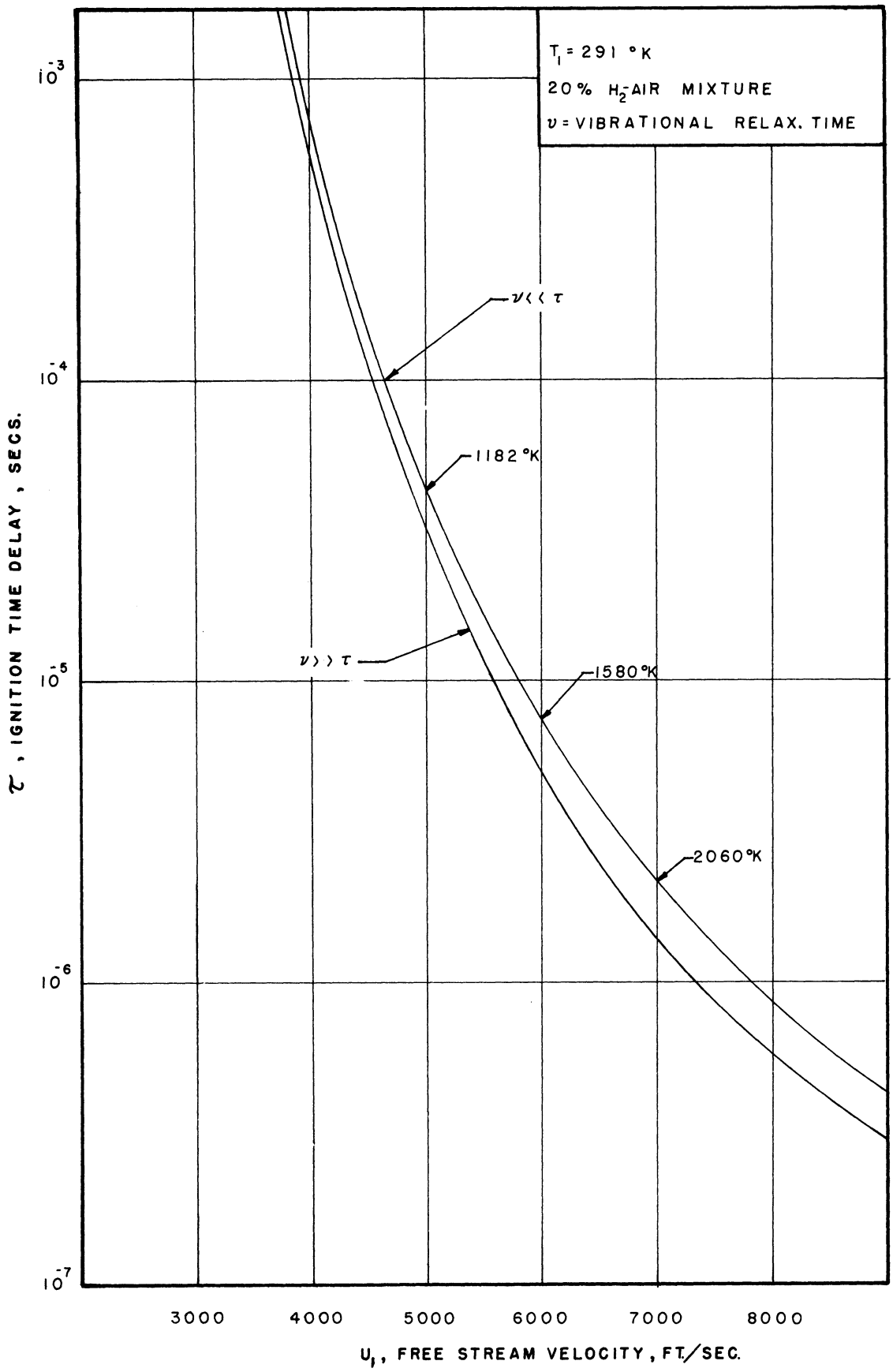

Fig. 10. Ignition time delay as a function of free stream velocity, with and without vibrational relaxation behind normal shock, for 20% H_2-air mixture.

worthwhile to note that in the range of delays reported in this investigation (10-50 μsec) the difference amounts to approximately 25%. With the existing degree of uncertainty as to the value of the pertinent reaction rate constants, this difference is too small to conclude from the experiments whether vibration was fully excited or not.

VI. TWO-DIMENSIONAL EFFECTS

The correlation between the ignition time delay as evaluated from the theoretical Eq. (4.23) and the experimental distance between the Mach disc and the flame front is based on the assumption that the flow parameters and the molecular weight remain unchanged in the region immediately behind the Mach disc up to the flame front. Figure 7 shows that the experimental results (after having been reduced according to this assumption) have lower values than the theoretical predictions and that this discrepancy increases at the lower temperatures behind the shock (T_2).

It has been previously stated[2] that the discrepancy could be due to two dimensional effects. A quantitative evaluation of this effect is the object of this section.

The main assumption to be made here is that the flow immediately behind the Mach disc diverges and that the angle of divergence remains constant for all ranges of ignition time delay. Thus the two-dimensional effect becomes that of finding the effect of increasing flow area on the theoretical delay distance. From the expression of the ignition delay time, Eq. (4.23), and the velocity behind the shock, the expression for the theoretical delay distance, Δx_t, is

$$\Delta x_t = \frac{RT_2}{2n_{O_2}P_2A_6} e^{E_6/RT_2} \ell n \left(\frac{n_{O_2}}{n_{H_2}} \cdot \frac{k_6}{k_5} \right) M_2 \sqrt{\gamma RT_2} \qquad (6.1)$$

where M_2 is the Mach number behind the shock. Inasmuch as a change in area

is assumed, the temperature and pressure and Mach number change with distance from the shock front. Thus Δx_t is a function of the three variables, P_2, T_2, and M_2. Taking the logarithm of Eq. (6.1) and differentiating we obtain

$$\frac{d(\Delta x_t)}{\Delta x_t} = \left(\frac{3}{2} - \frac{E_6}{RT_2}\right)\left(\frac{dT_2}{T_2}\right) - \frac{dP_2}{P_2} + \frac{dM_2}{M_2} \tag{6.2}$$

where the logarithm term of (6.1) has been taken as a constant. Since the flow is subsonic behind the shock, an area increase increases both the static temperature and the static pressure and decreases the Mach number and since $E_6/RT_2 > 3/2$ in the range of temperature of interest here, an area increase reduces the delay distance.

Now, dT_2/T_2, dP_2/P_2 and dM_2/M_2 can be evaluated in terms of M_2 and dA/A by using the influence coefficients (Ref.17, p. 228, Table 1). Making the substitution we obtain

$$\frac{d(\Delta x_t)}{\Delta x_t} = \left[\left(\frac{3}{2} - \frac{E_6}{RT_2}\right)(\gamma-1)M_2^2 - \gamma M_2^2 - \left(1 + \frac{\gamma-1}{2} M_2^2\right)\right] \frac{1}{1 - M_2^2} \frac{dA}{A} \tag{6.3}$$

With the value of $E_6/RT_2 = 8.2$ corresponding to $T_2 = 1100°K$, it can readily be seen that $\frac{d(\Delta x_t)}{\Delta x_t}$ varies between -1.945 dA/A and -1.05 dA/A as M_2 varies between .4 and .1, so that as an average one can write

$$\frac{d(\Delta x_t)}{\Delta x_t} \cong -1.5 \frac{dA}{A} \tag{6.4}$$

This equation can be written in incremental form in terms of the experimental delay distance, Δx, the divergence angle, δ, and the Mach disc radius, r_d, as follows:

$$\frac{\Delta x_t - \Delta x}{\Delta x_t} \cong \frac{3\Delta x \tan \delta}{r_d} \tag{6.5}$$

when $\Delta x \tan \delta \ll r_d$. It shows that the fractional deviation between the theoretical and the experimental delay distances decreases with increasing radius of the Mach disc and decreasing delay distance. Thus the larger the scale of the experiment and the higher the temperature the better the agreement is between experiment and theory.

It remains now to evaluate tan δ. To do this, the results of run No. 31 which seems to give the closest agreement with theory are used. Admittedly, the values for the theoretical curve are not that well-known to justify superimposing the two but it is the best we can do here to assess the two dimensional aspects. Evaluating Δx_t from Eq. (6.5) and noting that $r_d \cong .25$ in., tan δ is found to be .145 corresponding to $\delta = 8.25°$. Although this angle appears to be relatively large, it should be pointed out that the observed divergence angle of the flame is about twice this value, therefore $\delta = 8.25°$ is considered reasonable. With the value of δ thus obtained, it is possible to correct all the other experimental distances and thus evaluate τ_t, the corresponding theoretical time delay. Figure 11 shows a comparison between the corrected experimental results and theory and it can be seen that the agreement is extremely good. Most of the corrected experimental points lie within ±25% of the theoretical curve. Thus the above, admittedly somewhat crude, analysis indicates that two dimensional effects are of importance in the case of longer delays and serve to explain the results observed.

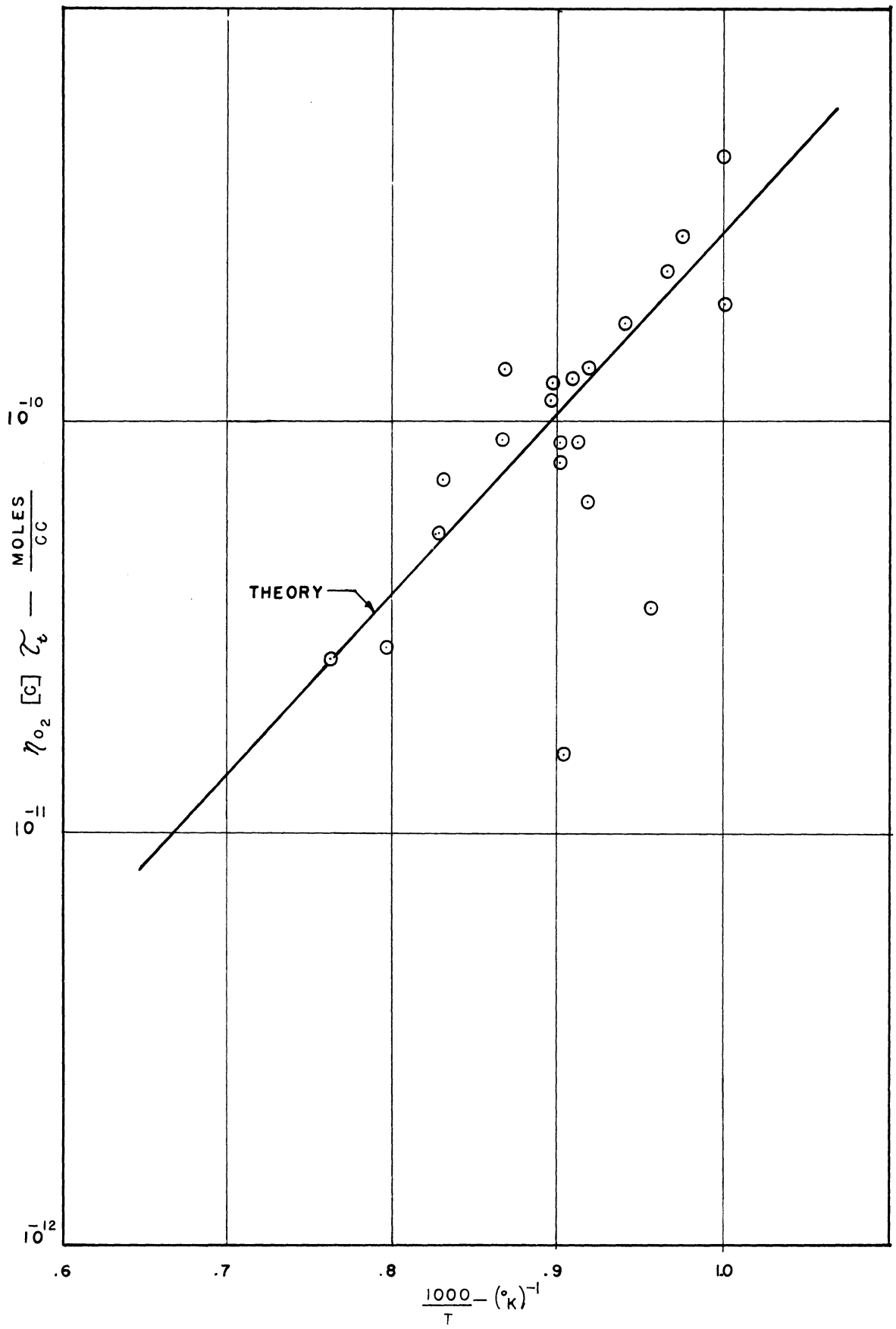

Fig. 11. Comparison of theoretical and experimental time delays (with two-dimensional effects correction) for H_2-air mixtures.

VII. MAGNETOGASDYNAMIC EFFECTS ON PLANE, GASEOUS DETONATION WAVES

INTRODUCTION

The relatively high degree of ionization which can exist behind strong normal shock and detonation waves has prompted several investigators to examine the possibility of affecting the properties of these waves by the application of hydromagnetic forces. Among these investigations is the work of Gross, Chinitz, and Rivlin,[18] and Landau and Lifschitz[19] and Gourdine.[20] The latter author is the only one who has treated waves behind which exist a gas with finite electrical conductivity. References 18 and 19 take up the case of infinite conductivity; a not too realistic situation unless the shock is extremely strong or the flow behind it is heavily seeded. Furthermore, Gourdine assumes that the effects of hydromagnetic forces are confined to a region throughout which all properties are uniform. In the present treatment part of this restriction has been removed and the variation of properties i.e., temperature, velocity, etc., throughout the aforementioned region is determined by the generalized one-dimensional flow methods of Shapiro.[17] The final results, however, are in the familiar form of difference equations wherein the flow variables far downstream of the discontinuity/ interaction region are determined entirely by the upstream variables, the bulk heat addition, and the degree of hydromagnetic interaction. The latter influence is characterized by a parameter which expresses the ratio of hydromagnetic forces to dynamic forces in the fluid.

FORMULATION OF A MODEL

In order to render such a problem tractable to analysis many simplifying assumptions must be made. A first, and not at all limiting assumption, is that the flow is strictly one-dimensional. Upstream of the discontinuity the electrical conductivity is zero and the unshocked gas, therefore, is not subject to magnetogasdynamic forces; even though a magnetic and velocity field may exist in that region. Next, the thickness of the discontinuity as well as the zone of heat addition (chemical energy release) is negligibly small compared to the length of the magnetic interaction region. The length of the interaction region can be controlled and made finite by, say, shorting out magnetic flux lines with a ferromagnetic shield so that they may not extend downstream of this point. Finally, in the interaction region, the electrical conductivity, σ, and the magnetic flux density, B, are assumed to be constant and capable of being arbitrarily specified. As is usual in problems involving a small electrical conductivity the magnetic Reynolds number is likewise small, implying no induced magnetic field. There is no electric field either induced or applied and the problems of closure of current lines and the pressure of non-conducting walls are ignored. Since no electric field exists there will be no magnetogasdynamic terms in the energy equation and the conservation relations are simply

$$\rho u \frac{du}{dx} = - \frac{dP}{dx} - \sigma u B^2 \tag{7.1}$$

$$\frac{d}{dx}\left(C_p T + \frac{u^2}{2}\right) + \frac{d}{dx} Q = 0 \tag{7.2}$$

$$\frac{d}{dx} (\rho u) = 0 \tag{7.3}$$

Equations (7.1-7.3) express the conservation of momentum, energy, and mass respectively in a one-dimensional flow. The term involving the electrical conductivity in Eq. (7.1) is the Lorentz force term and Q represents bulk heat addition in Eq. (7.2). It will be assumed the fluid behaves as a perfect gas with the same C_p and γ on either side of the discontinuity. Consider the following sketch:

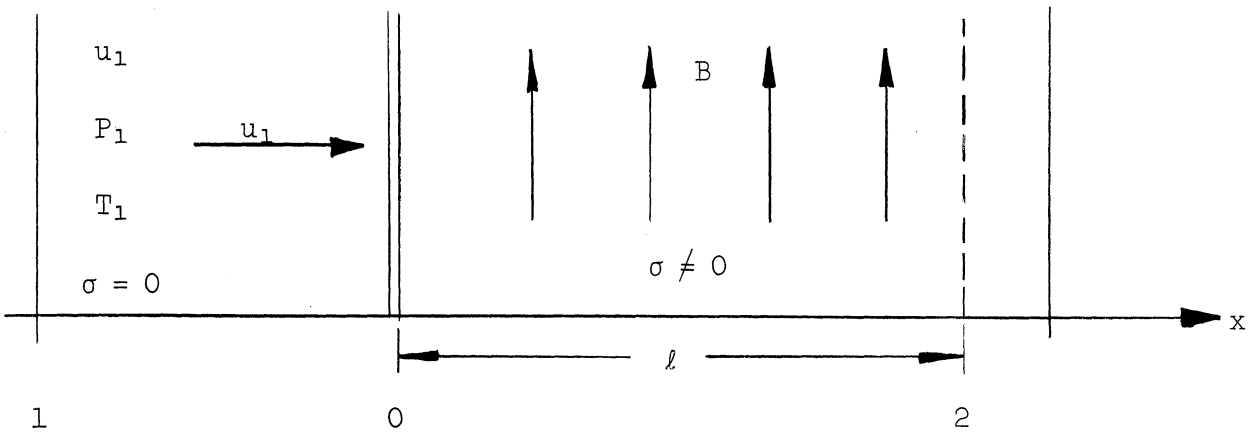

Integrating Eqs. (7.1-7.3) between stations 1 and 2 one obtains:

$$\rho_2 u_2^2 - \rho_1 u_1^2 + (P_2 - P_1) + \int_1^2 \sigma u B^2 \, dx = 0 \tag{7.4}$$

$$C_p T_1 + \frac{u_1^2}{2} + Q = C_p T_2 + \frac{u_2^2}{2} \tag{7.5}$$

$$\rho_1 u_1 = \rho_2 u_2, \quad P_2 = \rho_2 R T_2 \tag{7.6}$$

Now the region upstream of station 0 will contribute nothing to the integral in Eq. (7.4) and it may therefore be written as

$$F = \int_0^{\ell} \sigma u B^2 \, dx = \sigma B^2 \int_0^{\ell} u \, dx \tag{7.7}$$

the second form following from the assumption of constant conductivity and magnetic filed in the interaction region. One can see that the problem now consists of merely evaluating the integral, Eq. (7.7). The technique adopted is that the interaction region is analyzed separately from the discontinuity and then conditions are matched at station 0. This is much the same approach that is used in the analysis of a detonation wave; a shock followed by combustion.

ANALYSIS OF MODEL

In order to evaluate the integral, (7.7), it will be necessary to find the variation of the velocity, u, throughout the region of interaction. Such a problem can be solved by the one-dimensional flow techniques of Shapiro.[17] The Lorentz force is treated as a general body force and from Ref. 17 one finds

$$\frac{dM^2}{M^2} = \frac{M^2}{(1 - M^2)} \left[1 + \frac{\gamma-1}{2} M^2\right] \frac{dX}{\frac{1}{2} \gamma PAM^2} \tag{7.8}$$

where dX is a differential body force and $\frac{1}{2} \gamma PAM^2$ is the dynamic pressure in the flow. A word about the definition of Mach number is in order at this point. In a conducting gas permeated by a magnetic field the speed of small disturbances is

$$b^2 = a^2 + A_o^2$$

where "a" is the ordinary gas dynamic sound speed and A_o is the speed of propagation of transverse disturbances known as the Alfven speed. This composite speed may be rewritten as

$$b = \sqrt{\gamma RT + \frac{\mu_o H^2}{\rho}}$$

where μ_o is the permeability of free space (MKSQ units are employed throughout). One often speaks of a magnetic pressure defined as

$$P_{mag} = \frac{\mu_o H^2}{2}$$

and in terms of this variable

$$b = a\sqrt{1 + \frac{2P_{mag}}{\gamma P}}$$

Behind a strong shock or detonation it will be permissible (as will be shown later) to assume

$$\frac{2P_{mag}}{\gamma P} \ll 1$$

in consequence of which

$$b \cong a.$$

Then the Mach number has its usual definition

$$M = \frac{u}{a}.$$

Since the expression for the differential Lorentz force is

$$dX = \sigma u B^2 A\, dx$$

one sees immediately that

$$\frac{dX}{\frac{1}{2}\gamma P A M^2} = \frac{2\sigma B^2\, dx}{(\rho u)}.$$

According to the continuity Eq. (7.6), (ρu) is a constant of the flow. In Ref. 21, Patrick and Brogan, who have treated a similar problem, introduce a variable S defined by the relation

$$dS = \frac{\sigma B^2 \, dx}{(\rho u)}$$

This new variable is nothing more than the ratio of Lorentz forces to dynamic forces and is sometimes referred to in the literature as Q. Now rewrite Eq. (7.8) using this new variable and obtain

$$\frac{dM^2}{M^2} = \frac{2\gamma M^2}{1 - M^2} \left(1 + \frac{\gamma - 1}{2} M^2\right) dS$$

Integrating the above from S = 0 and M = M_o yields

$$2\gamma S = \left[\left(\frac{1}{M_o^2} - \frac{1}{M^2} \right) + \frac{\gamma + 1}{2} \ell n \left(\frac{M_o^2}{M^2} \, \frac{1 + \frac{\gamma - 1}{2} M^2}{1 + \frac{\gamma - 1}{2} M_o^2} \right) \right] \tag{7.9}$$

Of particular interest is the case when M = 1 or choking occurs at station 2. Equation (7.9) then, yields a unique relationship between S_{max} and M_o^2 which is perfectly analogous to the case of frictional flow in a pipe with a maximum allowable length. Here the interaction parameter can be no more than S_{max} for a given M_o (and, of course, γ) or a change in upstream conditions will result. The behavior of S_{max} for $\gamma = 1.4$ is shown in Fig. 12. Having obtained the variation of Mach number in the interaction region one can now find the velocity variation. First find $u(M^2)$ from

$$\frac{du}{u} = \frac{\gamma M^2}{1 - M^2} dS = \frac{\gamma M^2}{1 - M^2} \left(\frac{dS}{dM^2} \right) dM^2$$

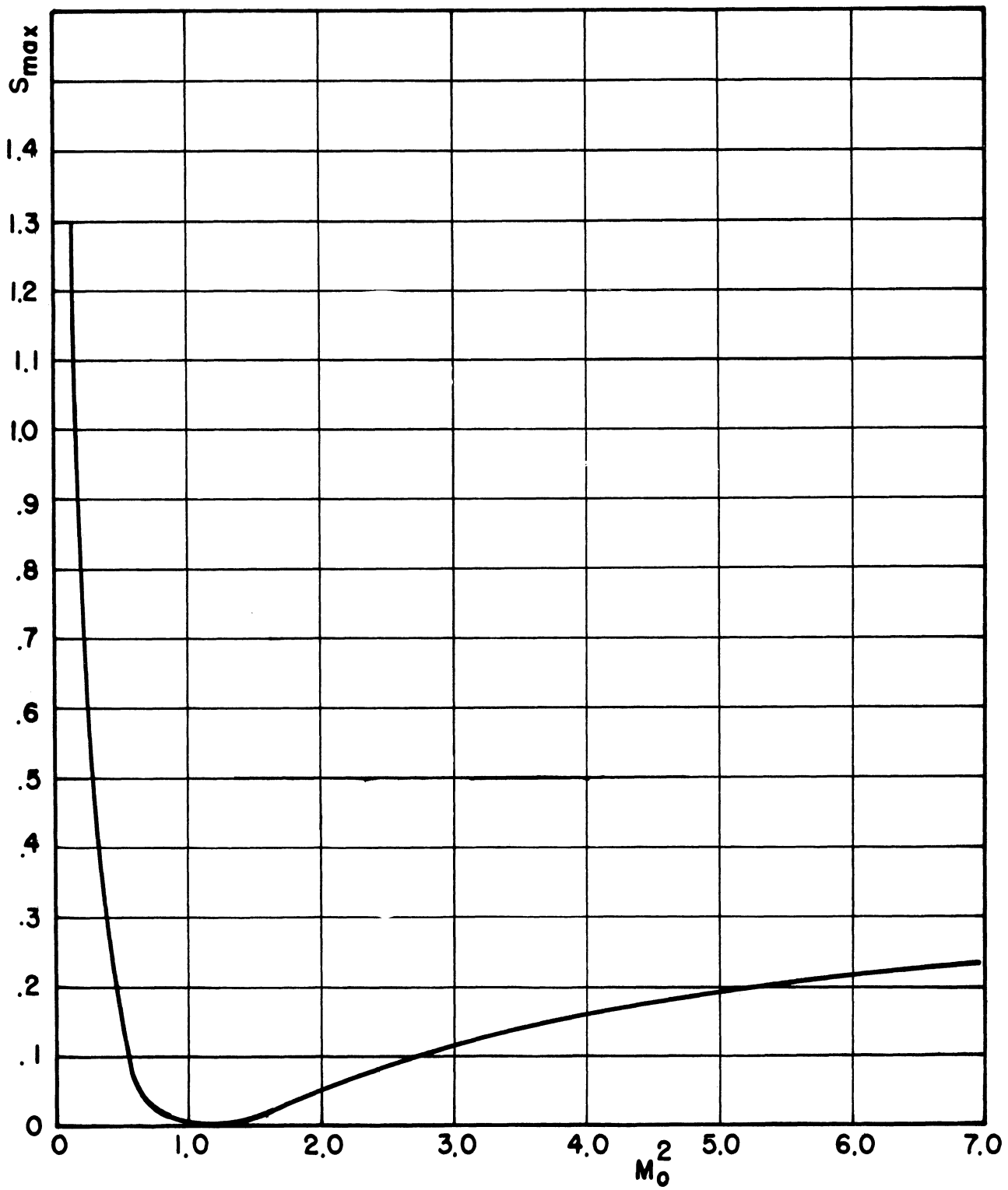

Fig. 12. Plot of S_{max} as a function of M_o^2 according to Eq. (7.9) when M = 1.

Inserting the value for dS/dM^2 into the above expression yields

$$2\frac{du}{u} = \frac{dM^2}{M^2\left(1 + \frac{\gamma-1}{2} M^2\right)}$$

Integrating from u_o and M_o gives

$$\bar{u}^2 = \frac{M^2}{M_o^2} \frac{1 + \frac{\gamma-1}{2} M_o^2}{1 + \frac{\gamma-1}{2} M^2}$$

where

$$\bar{u} = \frac{u}{u_o} .$$

Solving for M^2 in terms of $\bar{u}^2$ and inserting the result into Eq. (7.9) gives the expression

$$2\gamma S = \left(\frac{\bar{u}^2 - 1}{\bar{u}^2}\right)\left(\frac{1 + \frac{\gamma-1}{2} M_o^2}{M_o^2}\right) - \frac{\gamma+1}{2} \ell n\,(\bar{u}^2) \qquad (7.10)$$

This type of one-dimensional flow behaves exactly like flows with simple heat addition or simple friction. If the initial Mach number, M_o, is less than unity the flow is accelerated while for $M_o > 1$ the flow is decelerated. The former case will apply for flow behind a normal discontinuity.

Now consider a recast form of the Lorentz force integral, Eq. (7.7). One can write

$$F = \frac{\sigma B^2 u_o(\rho u)}{\sigma B^2} \int_o^{S_\ell} \bar{u}\, dS = (\rho u) u_o \int_1^{\bar{u}_2} \bar{u}\left(\frac{dS}{d\bar{u}}\right) d\bar{u} \qquad (7.11)$$

From Eq. (7.10)

$$\bar{u}\frac{dS}{d\bar{u}} = \left(\frac{1 + \frac{\gamma-1}{2} M_o^2}{\gamma M_o^2}\right)\frac{1}{\bar{u}} - \frac{\gamma+1}{2\gamma}$$

Hence the integral is easily found to be

$$F = \frac{(\rho u)u_o}{\gamma}\left[\frac{1 + \frac{\gamma-1}{2}M_o^2}{M_o^2}\left(\frac{\bar{u}_2 - 1}{\bar{u}_2}\right) - \frac{\gamma+1}{2}(\bar{u}_2 - 1)\right] \qquad (7.12)$$

It may not be clear that the integrated force term is a function of conditions at x = 0 and of S_ℓ, only. However, reference to Eq. (7.10) which gives $\bar{u}$ as a function of S and M_o, will verify that this dependence does indeed exist.

Now for operation with the difference Eqs. (7.4-7.6), the term F/P_1 will be of importance. For convenience introduce the parameter

$$\lambda = \sqrt{\frac{1 + \frac{\gamma-1}{2}M^2}{\frac{\gamma+1}{2}M^2}}$$

and from the first equation for $\bar{u}^2$ obtain

$$\bar{u}_2 = \frac{\lambda_o}{\lambda_2}$$

Inserting this simplified notation into Eq. (7.12) gives the following expression for the integrated Lorentz force

$$F = \frac{\rho_o u_o^2}{\gamma}\left(\frac{\gamma+1}{2}\right)\left(\frac{\lambda_o - \lambda_2}{\lambda_2}\right)(\lambda_2\lambda_o - 1)$$

Now F/P_1 can be written as

$$F/P_1 = \frac{P_2}{P_1}\frac{\rho_o u_o^2}{\gamma P_2}\left(\frac{\gamma+1}{2}\right)\left(\frac{\lambda_o - \lambda_2}{\lambda_2}\right)(\lambda_2\lambda_o - 1) \qquad (7.13)$$

Using Shapiro's technique an expression for pressure as a function of Mach number can be obtained which can be put in the form

$$\left(\frac{P_2}{P_o}\right)^2 = \left(\frac{M_o^2}{M_2^2}\right)^2 \frac{\lambda_o^2}{\lambda_2^2}$$

Substituting for P_2 in the denominator of Eq. (7.13) (and noting $\rho_o u_o^2/\gamma P_o = M_o^2$) gives

$$\frac{F}{P_1} = \frac{P_2}{P_1} M_2^2 \left(\frac{\gamma+1}{2}\right)\left(\frac{\lambda_o - \lambda_2}{\lambda_o}\right)(\lambda_2\lambda_o - 1) \tag{7.14}$$

Now by dividing Eq. (7.4) by P_1 one can obtain

$$\frac{P_2}{P_1}\gamma M_2^2 - \gamma M_1^2 + \frac{P_2}{P_1} - 1 + \frac{F}{P_1} = 0$$

Solving for P_2/P_1 gives the result

$$\frac{P_2}{P_1} = \frac{(1 + \gamma M_1^2)}{1 + M_2^2\left[\gamma + \left(\frac{\gamma+1}{2}\right)\left(\frac{\lambda_o - \lambda_2}{\lambda_o}\right)(\lambda_2\lambda_o - 1)\right]} \tag{7.15}$$

Likewise the energy integral, Eq. (7.5), may be cast into the form

$$\left(1 + \frac{\gamma-1}{2} M_1^2\right) + \frac{Q}{C_p T_1} = \left(\frac{P_2}{P_1}\right)^2 \left(\frac{M_2}{M_1}\right)^2 \left(1 + \frac{\gamma-1}{2} M_2^2\right)$$

Setting $Q/C_pT_1 = \bar{Q}$ and using Eq. (7.15) for P_2/P_1 one finally obtains a relation between M_1 and M_2 with S_ℓ as an (implicit) parameter, thus

$$\frac{M_1^2\left(1 + \frac{\gamma-1}{2} M_1^2\right) + \bar{Q}}{(1 + \gamma M_1^2)^2} = \frac{M_2^2\left(1 + \frac{\gamma-1}{2} M_2^2\right)}{\left[1 + M_2^2\left(\gamma + \frac{\gamma+1}{2}\,\frac{\lambda_o - \lambda_2}{\lambda_o}\,(\lambda_2\lambda_o - 1)\right)\right]^2} \tag{7.16}$$

In order to find M_2 from Eq. (7.16) it is necessary to specify only M_1, $\bar{Q}$, and the interaction parameter, S_ℓ.

THE PSEUDO-CHAPMAN-JOUGUET SOLUTION

For the special case when $M_2 = 1$ one can think of Eq. (7.16) as yielding a pseudo-Chapman-Jouguet solution. It is only a formal comparison and the

singularity of such a solution has not been examined. For $M_2 = 1$, $\lambda_2 = 1$ and Eq. (7.16) becomes

$$\frac{M_1^2\left[\left(1 + \frac{\gamma-1}{2} M_1^2\right) + \bar{Q}\right.}{(1 + \gamma M_1^2)^2} = \frac{2\lambda_o^2}{(\gamma+1)(\lambda_o^2 + 1)^2} \qquad (7.17)$$

If one defines

$$\beta = \frac{2\lambda_o^2}{(\gamma+1)(\lambda_o^2 + 1)^2},$$

Eq. (7.17) may be solved for M_1^2 resulting in

$$M_1^2 = \left[\frac{(1 - 2\beta\gamma) + \bar{Q}}{1 - 2\gamma(1 - 2\beta\gamma)}\right]\left\{1 + \sqrt{1 - \frac{2\beta[1 - \gamma(1 - 2\beta\gamma)]}{[(1 - 2\beta\gamma) + \bar{Q}]^2}}\right\} \qquad (7.18)$$

Here it should be remembered that M_1 is related to S_ℓ, the interaction parameter, through β and hence λ_o^2. Since $M_2 = 1$ there is a unique value of λ_o for each value of S_ℓ as can be seen from Fig. 12. One may select a value of $\bar{Q}$ and a value of S_ℓ and proceed to calculate M_1 from Eq. (7.18). This has been done for an appropriate range of variables and the results are shown in Fig. 13.

Now a word about the coordinate system used in this analysis is in order. It has been assumed that the magnetic field is fixed relative to the detonation wave. Then if the wave is stationary in laboratory coordinates, Fig. 13 simply shows what Mach number must exist upstream of the discontinuity in order that $M_2 = 1$ exists at the end of the interaction region. If the detonation wave moves in laboratory coordinates then Fig. 13 gives the Mach number

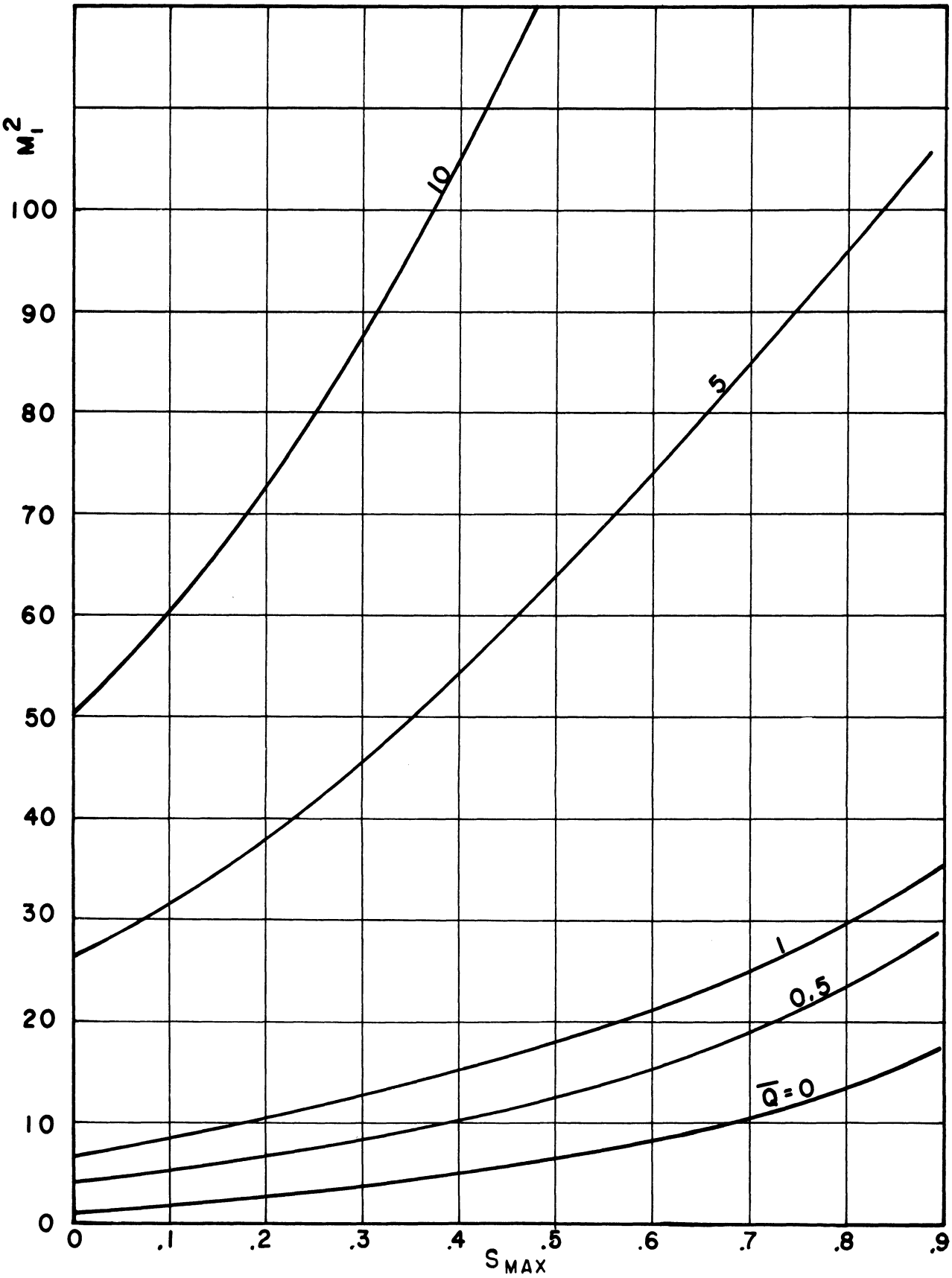

Fig. 13. Propagation Mach number as a function of S_{max} with heat addition as parameter.

of propagation implying, of course, that the magnetic field is moving at the same speed. In the latter case the moving field is accelerating the wave to a greater speed than it would attain on the basis of chemical and mechanical energy considerations alone. For the stationary wave the magnetic field acts as an agent to convert kinetic energy to thermal energy via Joulean dissipation. Considering the case where the field acts as an accelerating mechanism, Fig. 13 shows that the effectiveness of the field in this role is enhanced by bulk heat addition. The uppermost curve, for $\overline{Q} = 10$, represents a situation achieved by many oxygen-hydrocarbon detonations. The present analysis shows that it should be possible to increase the detonation Mach number by more than a factor of two for $S_\ell \cong 0.5$. In order to produce such a value of S_ℓ will require (P_1 = 1 ATM, T_1 = 70°F) any combination of variables which satisfies the equality

$$\sigma B^2 \ell = 2.3.$$

Thus if σ = 10 mhos/meter (extremely reasonable) and a flux density of .5 webers/sq meter (5000 gauss) exists, the interaction length need be only .92 meters for the equality to be satisfied. All of these values are modest and easily achievable; hence laboratory verification of the analytical predictions should not be too difficult.

Now consider again the assumption made previously concerning the speed of small disturbances in a conducting gas permeated by a magnetic field. It was stated that for $2P_{mag}/\gamma P \ll 1$ one could define the Mach number in the usual way. For the numerical example considered above Eq. (7.15) shows

$$P_2/P_1 \cong 61$$

Since a B of 0.5 webers/sq meter corresponds to a "magnetic pressure" of about 1 atmosphere the inequality

$$\frac{2P_{mag}}{\gamma P_2} \cong .021 \ll 1$$

is easily satisfied. For this condition, at least, the assumption is valid. For most of the range of variables shown in Fig. 13 the assumption is valid and only for very weak shock waves will it be invalid.

VIII. LINEARIZED THEORY OF SUPERSONIC COMBUSTION

INTRODUCTION

There is currently an intense interest in the development of very high Mach number ramjets. At these high Mach numbers it is advantageous to maintain a supersonic flow through the combustor. Some consideration has thus been given to detonative combustion but it appears that shock free combustion in a supersonic stream would lead to better performance if it can be obtained. One would suspect that the prospects of avoiding strong shocks would be enhanced if the combustion could occur gradually and hence a linearized analysis would be of value. Linearized analyses have also been applied to the external combustion airfoil wherein heat addition to the supersonic stream causes an increase in pressure which can result in net lift and thrust. Such a scheme appears attractive for maneuverability at high altitudes.

In the interest of checking the validity of the linearized treatment of supersonic combustion, it was decided to perform some novel preliminary experiments. It was felt that adding heat to the stream under a flat plate airfoil by means of a number of very small heated wires would circumvent the problems of fuel injection and thus give a more critical check on the theoretical predictions.* Such experiments were initiated, the results of which are reported in the ensuing sections.

*This idea was suggested by Dr. Raymond Kushida of the National Engineering Sciences Co.

THEORETICAL ANALYSIS

Various authors,[22-25] have analyzed combustion under a two-dimensional wing by means of linearized theory. Following the analysis of Ref. 23, the heat addition is confined between the forward facing Mach waves emanating from the lower trailing surface of the wing and the leading edge and is assumed to take place outside the boundary layer in the supersonic stream. The effects of viscosity and heat conduction are neglected and the flow is assumed to be irrotational and behaves as a perfect gas. As for the wing, it is assumed to be a flat plate operating at zero angle of attack. On the basis of these assumptions the following relationship between the lift and heat added, L/Q, is found from the potential flow equations:

$$\left(\frac{L}{Q}\right)_{\alpha=0} = \frac{\gamma-1}{a} \frac{M}{\sqrt{M^2 - 1}} \tag{8.1}$$

where

γ = ratio of specfic heats

M = Mach number

a = speed of sound

EXPERIMENTAL PROCEDURE

Equation (8.1) shows that the lift is independent of the intensity and distribution of the heat addition, as long as it is small. On the basis of these conclusions and the simplicity of Eq. (8.1) it was decided to set up an experiment which would check the validity of the linearized theory for underwing heat addition.

To check the linearized theory there are two major quantities that we wish to measure. One, is the lift L, and other the heat release Q. With these two quantities measured experimentally, and knowing the flight Mach number of the wing; $(L/Q)_{experimental}$ can be compared with $(L/Q)_{theory}$. Let us begin then, by examining the lifting device and its characteristics.

A flat plate at zero angle of attack was chosen due to the simplicity involved in calculating the lift. For a flat plate at zero angle of attack the lift is

$$L_{total} = \ell \int_0^c \Delta P dx \qquad (8.2)$$

where

ℓ = span

P = pressure differential between upper and lower surfaces

C = chord

By measuring ΔP at various chordwise stations along the flat plate the lift with and without heat addition can be calculated by Eq. (8.2) using numerical integration. In this way, the increment of lift due only to heat addition is known accurately.

The flat plate which was used had a chord length of 6 inches and a span of 4 inches with 20 chordwise pressure taps, 10 at center span and 10 at 1/4 span. The model was placed in The University of Michigan 4 x 7 inch supersonic wind tunnel which has a Mach number range of 1.5 to 4.5.

Before considering the method for attaining the heat release, Q, and its measurement, it is important to know the amount of heat release needed to produce a finite change in the lift. Assuming standard conditions, $(L/Q)_{theory}$

can be computed for various flight Mach numbers with the results shown in Fig. 14. From this figure for a given amount of heat added, the smallest measurable lift is where the curve is a minimum. This occurs at M = 1.9 where $(L/Q)_{theory}$ is .415. Using this as the design point and specifying at least a mean pressure rise of 4 inches of water, to be achieved by heat addition, the minimum amount of heat that can be added to the stream for accurate results is 5.55 Btu/sec. On this basis, one can proceed to the method of adding heat to a supersonic stream.

Two methods of adding heat to a supersonic stream were considered; chemical and electrical. The chemical method of squirting fuel through the airfoil for ignition and burning was neglected due to the nonlinear disturbances which would be present, hence electrical means were used to produce the heat addition. The method was to use I^2R heating from a finite number of thin wires placed span-wise under the flat plate. By placing the wires in the region of influence and measuring the current and voltage under steady state operation, the amount of heat Q added to the stream, can be determined from

$$Q = EI \tag{8.3}$$

where

E = volts

I = current

The next step is to consider the number of wires necessary to produce at least 5.55 Btu/sec. To do this, consider Kings equation[5]

$$Q = nNu_o \pi \ell (T_W - T_o) k_o \tag{8.4}$$

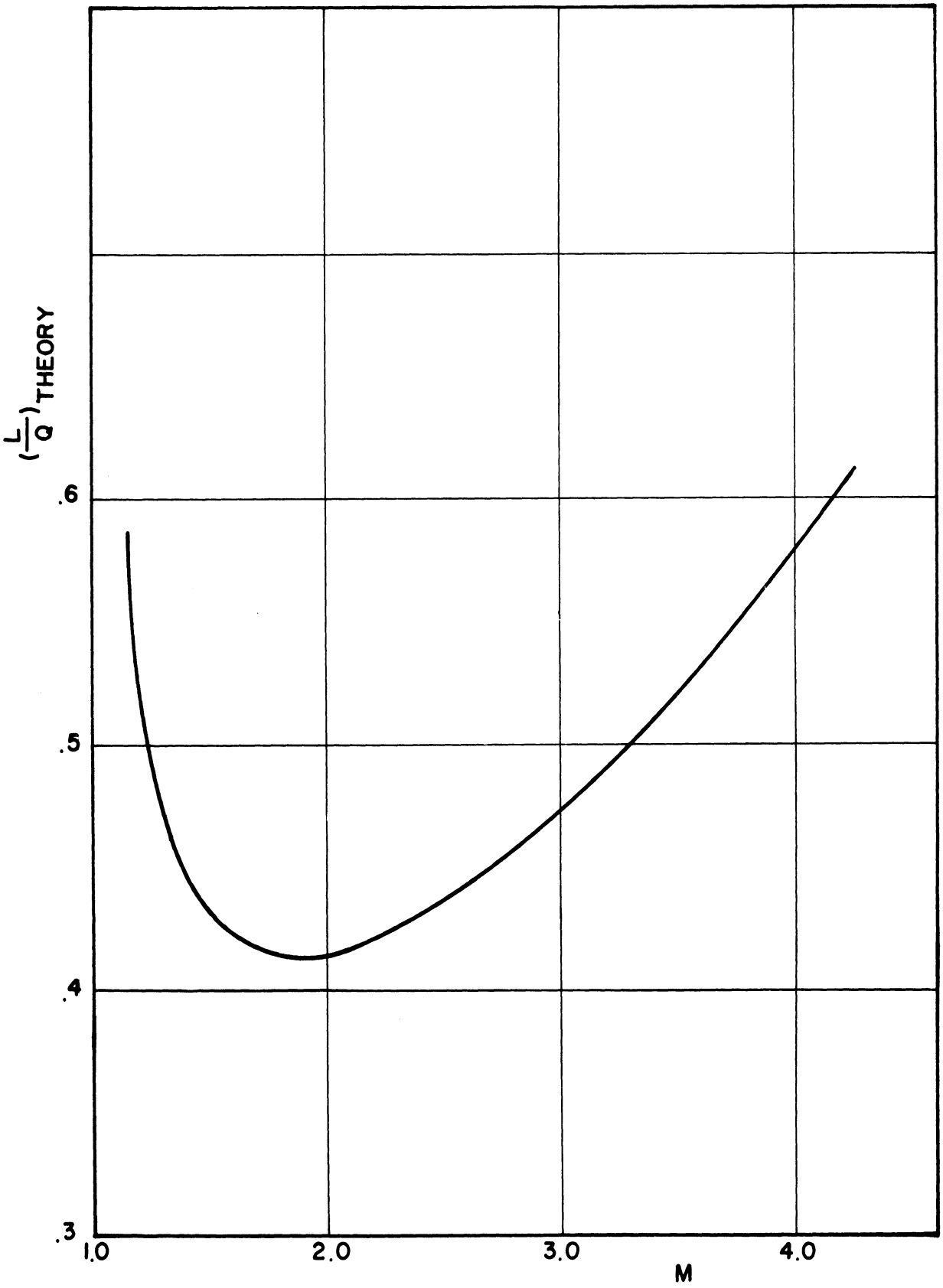

Fig. 14. Theoretical lift to heat addition ratio vs. free stream Mach number.

where

n = number of wires

Nu_o = Nusselt number = $0.580\sqrt{Re} - 0.795$

Re = Reynolds number

ℓ = length of one piece of wire

T_w = wire temperature

T_o = free stream stagnation temperature

k_o = heat conductivity

If we combine this with Eq. (8.1) using the relationship that

$$\frac{a}{a_o} = \frac{1}{\left(1 + \frac{\gamma-1}{2} M^2\right)^{1/2}}$$

we have

$$L = nNu_o \pi \ell (T_w - T_o) k_o \frac{(\gamma-1)}{a_o} \left(1 + \frac{\gamma-1}{2} M^2\right)^{1/2} \frac{M}{(M^2 - 1)^{1/2}} \qquad (8.5)$$

Simplifing Eq. (8.5), yields

$$\frac{L}{n} \lambda = Nu_o (T_w - T_o) \left[\frac{1 + \frac{\gamma-1}{2} M^2}{M^2 - 1}\right]^{1/2} M \qquad (8.6)$$

where

$$\lambda = \frac{a_o}{(\gamma-1) \pi \ell b_o}$$

Equation (8.6) can now be plotted against Mach number for various steady state wire temperatures as is done in Fig. 15. The wire used was Chromel "A" with a diameter of .02 inches.

With the use of Fig. 15 and the assumption that the steady state wire temperature is in the order of 2000°R, we can determine the number of wires

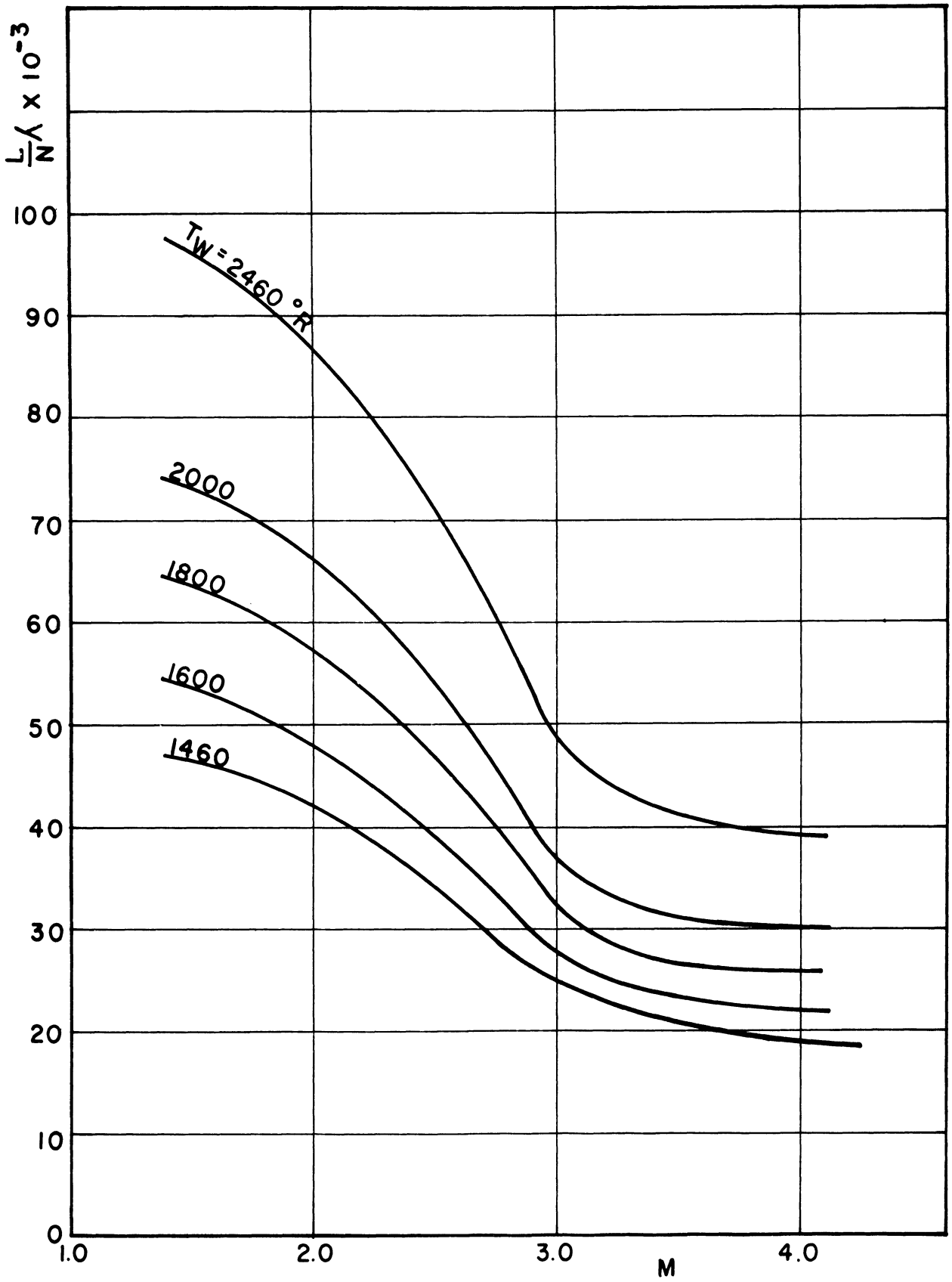

Fig. 15. Plot of $\frac{L}{n}\lambda$ against free stream Mach number [Eq. (8.6)].

necessary to produce the minimum Q of 5.55 Btu/sec. On this basis, the number of wires needed is 35.

Since Eq. (8.1) does not depend on the intensity of the heat addition it was decided to place the 35 wires in the region of influence for Mach number 3. In this way, as the experimental conditions were varied from Mach number 3 to Mach number 1.5, the wires would always be in the region of influence. The wire arrangement below the flat plate is shown in Fig. 16.

The last step before the experiment could be run was to determine the electrical requirements that would produce the necessary heat release. For the minimum heat release of 5.55 Btu/sec it was found that by using a parallel electrical circuit the current per wire would have to be 13.5 amperes with a total voltage of 10.9 volts. A bank of six heavy duty batteries was used as the electrical supply.

EXPERIMENTAL RESULTS

The experiment was first run with just the flat plate in the wind tunnel. This was done to insure that the change in pressure (i.e., P_o-P) was zero on the flat plate. Also, it was important that the manometer board and all associated equipment were working properly.

The next step was to insert the wires below the model and run with no heat addition. When this was done, the presence of the wires in the steam caused a boundary layer separation on the flat plate. The presence of the separation bubble was a disturbance which could not be considered within the assumptions of the linearized theory. At this point an attempt was made to

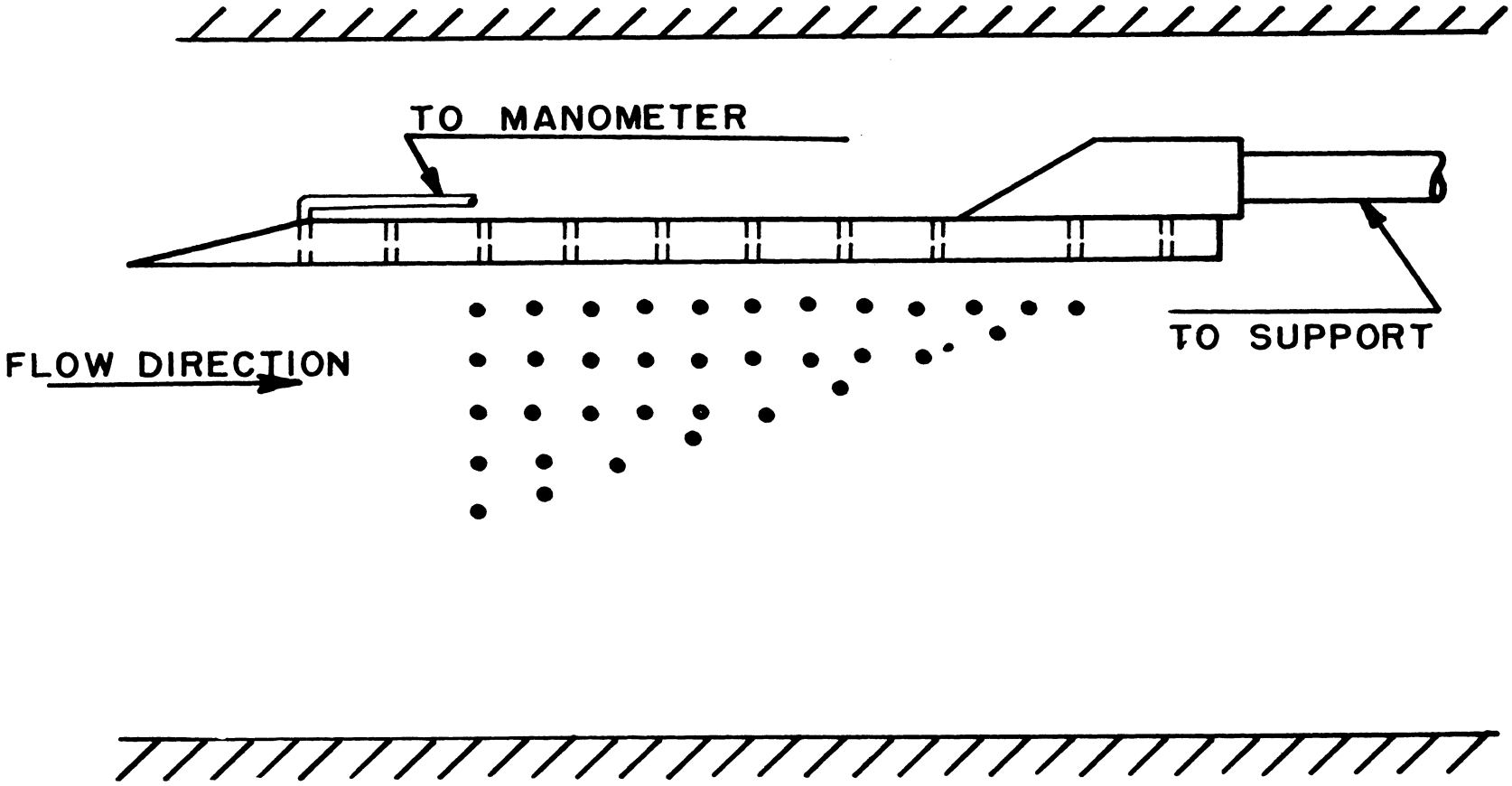

Fig. 16. Experimental arrangement of heating wires under flat plate.

eliminate the problem by making a study of the shock pattern from the wires. It was felt that the grouping of the wires was such that they caused a reinforcement pattern which caused the separation to take place on the flat plate. After studying the shock pattern, various wire patterns below the model in the region of influence were tried, none of which cured the separation problem. Time precluded further attempts to alleviate this problem and thus no conclusive results were obtained.

CONCLUSIONS

While the above preliminary experiments led to no conclusive check between experiment and theory, it is deemed worthwhile to pursue the investigation further. Conceivably the choice of other Mach numbers, different wire configurations, and boundary layer suction could alleviate the interaction problem. Also there is the possibility of adding the energy in other forms, such as by an electric arc or glow discharge or even by the condensation process. In order to avoid shocks it would seem that the energy addition would have to be gradual rather than abrupt.

IX. DISCUSSION

In Section II through VI the work performed under this contract relative to the study of standing detonation waves was reviewed. The experimental arrangement and technique was briefly described and some experimental results presented. In all cases observed, except when undesirable upstream burning was experienced, the combustion region was well separated from the shock wave. Consequently, a large effort was devoted to the study of the ignition delay zone. The results of the theoretical analysis were shown to be in quite good agreement with the experimental results, thus demonstrating the usefulness of the experimental procedure employed to the study of chemical kinetics. Refinements to these results were indicated by a treatment of vibrational relaxation and two-dimensional effects. While the observed ignition time delays would be appreciably affected by the two limiting cases of short or long vibrational relaxation times, the scatter in experimental results precluded a conclusion as to which of the two cases were realized (or, for that matter, whether the vibrational relaxation time was of the same order as the ignition time delay). It is believed that further experiments, conducted on a larger scale and wherein much more accurate measurements of the conditions behind the shock were effected, could be of great value in this regard.

Consideration of the two-dimensional effects realized in these studies showed that ignition delay was probably measureably affected. Here again an increase in the scale of the experiment would serve to minimize the effect.

To this point, nothing has been said about the interpretation of the experiments as regards strong or Chapman-Jouguet detonation. This facet has been discussed at length in an earlier publication.[26] In this reference the importance of the explosion limit criteria, the ignition delay distance, and the aerodynamic structure of the jet were considered in evaluating the results. It was concluded that under those conditions wherein the chemical energy was released close to the shock (relative to the dimensions of the jet), the resultant shock-combustion configuration could appropriately termed a detonation wave. With this definition some strong detonations were observed but in most cases the delay distance was too great to consider the phenomena detonation. This latter result is attributable to the limited temperatures available. In this same reference it was also concluded that transport processes were not important in the structure of the wave, at least not within the delay distance.

Much fundamental information can still be gained from a study of standing detonation waves. For example:

(a) larger scale experiments would permit exhaustive surveys of structure of the reaction zone in various mixtures;

(b) ignition delay times for other gases could be measured at high temperatures;

(c) the question of vibrational relaxation times and the influence of hydrogen on this time could be ascertained;

(d) the interaction between a seeded detonation wave and magnetic field should be investigated;

(e) the turbulence generated by a detonation wave could be assessed; and

(f) curved and oblique detonations stabilized by and on bodies could be studied.

Common to all of these studies mentioned is the prime requisite for higher temperatures. To date, so far as is known, no one has stabilized a gaseous detonation wave in an uncontaminated stream wherein the thickness of the wave is small compared to characteristic dimensions of the system. Higher stagnation temperature of the fuel-oxidant stream would permit this condition to be realized provided premature combustion can be avoided.

REFERENCES

1. Nicholls, J.A., Dabora, E.K., and Ong, R.S.B., "An Experimental Investigation of the Possibility of Achieving a Standing Detonation Wave," UMRI Report No. 2284-23-F, Ann Arbor, July 1959. Also issued as AFOSR TR 59-132.

2. Nicholls, J.A., "Stabilization of Gaseous Detonation Waves with Emphasis on the Ignition Time Delay Zone," UMRI Report No. 2874-6-T, Ann Arbor, June 1960. Also issued as AFOSR TN 60-442.

3. Nicholls, J.A., Dabora, E.K., and Gealer, R.L., "Studies in Connection with Stabilized Detonation Waves," Seventh Symposium on Combustion, London, Buttersworth Sci. Pub., 766 (1959).

4. Lewis, B., and von Elbe, G., Combustion, Flames and Explosions of Gases, New York Academic Press, Inc., 1951.

5. Physical Measurements in Gas Dynamics and Combustion, vol. IX, Princeton Series on High Speed Aerodynamics and Jet Propulsion, Princeton Univ. Press, 1954.

6. Buchele, D., A Self-Balancing Line-Reversal Pyrometer, NACA TN 3656, August, 1956.

7. Pearce, W.J., Plasma Jet Temperature Study, Aerosciences Lab., General Electric MSVD Report No. R59SD440, October, 1959.

8. Semenov, N.N., "Some Problems in Chemical Kinetics and Reactivity," II, Princeton Univ. Press, 1958.

9. Duff, R.E., "Calculation of Reaction Profiles Behind Steady-State Shock Waves. I. Application to Detonation Waves," The J. Chem. Phys., 28 (1958), 1193.

10. Schott, G.L., and Kinsey, J.L., "Kinetic Studies of Hydroxyl Radicals in Shock Waves. II. Induction Times in the Hydrogen-Oxygen Reaction," The J. Chem. Phys., 29 (1958), 1177.

11. Bethe, H.A., and Teller, E., "Deviations from Thermal Equilibrium in Shock Waves," Report No. X-117, Ballistic Res. Lab., Aberdeen Proving Ground, 1945.

12. Wood, G.P., "Calculations of the Rate of Thermal Dissociation of Air Behind Normal Shock Waves at Mach Numbers of 10, 12, and 14," NACA TN 3634, April 1956.

13. Patch, R.W., "Prediction of Composition Limits for Detonation and Hydrogen-Oxygen-Diluent Mixtures," ARS Journal, 31 (1961), 46.

14. Adamson, T.C., Jr., and Morrison, R.B., "On the Classification of Normal Detonation Waves," Jet Propulsion, 25 (1958), 400.

15. Hayes, W.C., and Probstein, R.F., Hypersonic Flow Theory, Academic Press, New York, 1959.

16. Liepmann, H.W. and Roshko, A., Elements of Gas Dynamics, John Wiley and Sons, Inc., 1957.

17. Shapiro, A.H., The Dynamics and Thermodynamics of Compressible Fluid Flow, vol. I, Ronald Press, New York, 1954.

18. Gross, R.A., Chinitz, W., and Rivlin, T.J., "Magnetohydrodynamic Effects in Combustion," J. Aero-Space Sci. Vol. 27, 283 (1960).

19. Landau and Lifschitz, Electrodynamics of Continuous Media, Addison-Wesley, 1960.

20. Gourdine, M.C., "The Effects of a Body-Force on Strong Shocks, Detonations, and Deflagrations," ARL-7-36, August 1957, Aero. Res. Lab., The Ramo-Wooldridge Corp., Los Angeles, California.

21. Patrick, R.M., and Brogan, T.R., "One-Dimensional Flow of an Ionized Gas Through a Magnetic Field," Journal of Fluid Mechanics, Vol. 5, Part 2, February 1959, p. 289.

22. Mager, Artur, "Supersonic Airfoil Performance with Small Heat Addition," IAS preprint 768 (1958).

23. Luidens, R.W., and Flaherty, R.J., "Analysis and Evaluation of Supersonic Underwing Heat Addition," NASA Memo 3-17-59E, April 1959.

24. Willmarth, W.W., "The Production of Aerodynamic Forces by Heat Addition on External Surfaces of Aircraft," Rand Report RM-2078, December 1957.

25. Gazely, Carl, Jr., "Linearized Solution for Heat Addition at the Surface of a Supersonic Airfoil," Rand Report RM-1892, November 1956.

26. Nicholls, J.A., and Dabora, E.K., "Recent Results on Standing Detonation Waves," 8th (International) Symposium on Combustion, California Institute of Technology, Pasadena, California, August 29-September 2, 1960. Also issued as AFOSR TN 60-441.